



# A review of additive manufacturing of metamaterials and developing trends

**Junxiang Fan<sup>1</sup>, Lei Zhang<sup>1</sup>, Shuaishuai Wei<sup>1</sup>, Zhi Zhang<sup>1</sup>, Seung-Kyum Choi<sup>2</sup>, Bo Song<sup>1\*</sup>, Yusheng Shi<sup>1</sup>**

<sup>1</sup> State Key Laboratory of Materials Processing and Die & Mould Technology, School of Materials Science and Engineering, Huazhong University of Science and Technology, Wuhan 430074, China

<sup>2</sup> George W. Woodruff School of Mechanical Engineering, Georgia Institute of Technology, Atlanta, GA 30332, USA

The concept of metamaterials originates from the proposal of left-hand materials with negative refractive index, followed by which, varieties of metamaterials with kinds of fantastic properties that cannot be found in natural materials, such as zero/negative Poisson's ratio, electromagnetic/acoustic/thermal cloaking effect, etc., were come up with. According to their application fields, the metamaterials are roughly classified into four categories, electromagnetic metamaterials, acoustic metamaterials, thermal metamaterials, and mechanical metamaterials. By designing structures and arranging the distribution of materials with different physical parameters, the function of metamaterials can be realized in theory. Additive manufacturing (AM) technology provides a more direct and efficient way to achieve a sample of metamaterial and experiment verification due to the great advantages in fabricating complex structures. In this review, we introduce the typical metamaterials in different application situations and their design methods. In particular, we are focused on the fabrication of metamaterials and the application status of AM technology in them. Furthermore, we discuss the limits of present metamaterials in the aspect of design method and the disadvantages of existing AM technology, as well as the development tendency of metamaterials.

**Keywords:** Metamaterials; Negative refractive index; Negative Poisson's ratio; Additive manufacturing

## Introduction

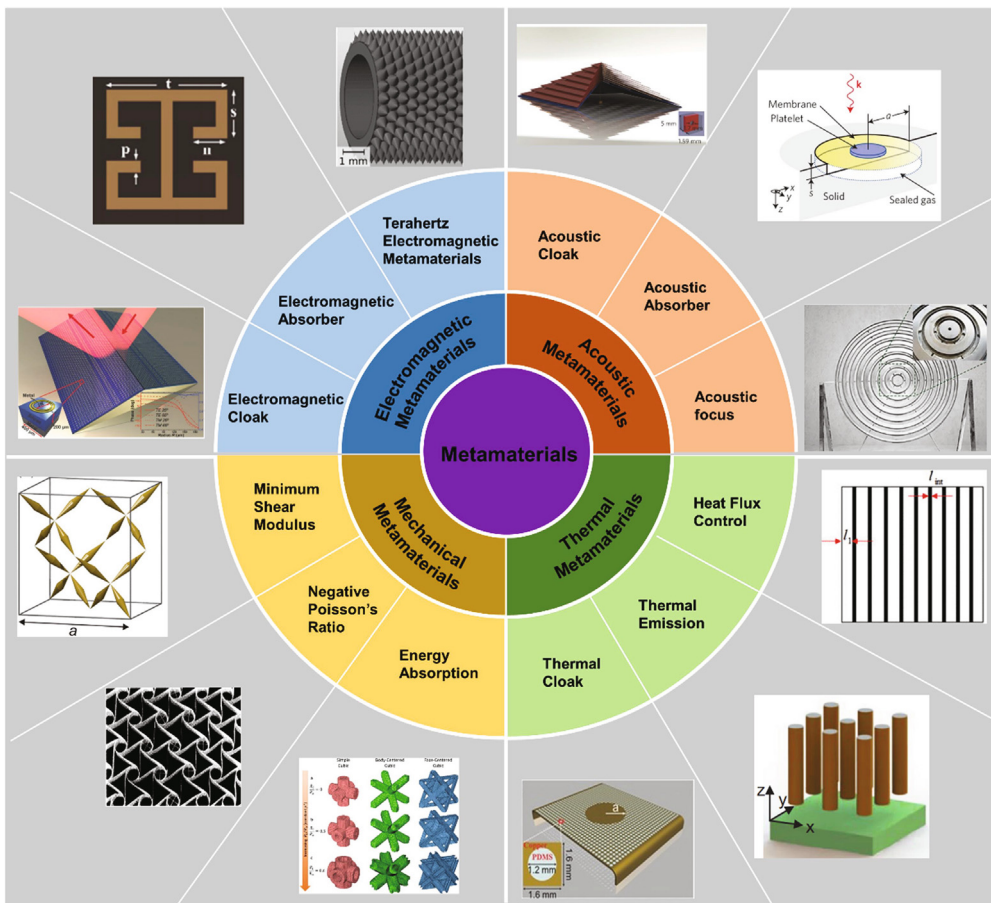
Metamaterials (MMs) refer to artificial structures or composite materials with extraordinary physical properties that can not be found in natural materials, such as electromagnetic/acoustic cloak [1–5], zero/negative Poisson's ratio [6–10], negative refractive index [11–15], etc. To realize these magic phenomena, some carefully designed structures with single material or multi-material were put forward, consisting of identical or gradually changing cell arrays. Similar to atoms or molecules in natural materials, these cells are basic units that determine the properties of MMs and are therefore called "artificial atoms". According to

their functionalities, currently developed MMs can be roughly classified into four categories: electromagnetic metamaterials (EMMs), acoustic metamaterials (AMMs), thermal metamaterials (TMMs), and mechanical metamaterials (MMMs), as shown in Fig. 1. All Acronyms and their corresponding meanings appeared in this review are summarized in Table 1 to make it more convenient for readers.

The research of MMs derived from the proposal of left-hand materials by Soviet physicist Veselago in 1968 [11], such materials would lead to many very interesting physical phenomena, such as negative refraction, electromagnetic stealth or absorption, etc. Another representative research achievement of EMMs is the proposal of the photonic crystal [16,17], in which electromagnetic waves of a certain frequency range could not propagate

\* Corresponding author.

E-mail address: Song, B. ([bosong@hust.edu.cn](mailto:bosong@hust.edu.cn))

**FIGURE 1**

The classification of MMs based on their functionalities.

because there was a photonic bandgap in their band structure, just like electronic bandgap in semiconductors. That made it promising in the fields of lasers and high-quality microwave antennas. However, before the structure of EMMs with negative permittivity and permeability was designed and manufactured [12,18], the research in this field only remained a theoretical hypothesis. Subsequently, the word “metamaterials” [19] was used to refer to those who achieved exotic performance beyond the limits of natural materials, and the concept was widely accepted. These exciting works attracted more and more researchers to devote themselves to the field of EMMs. Varieties of EMMs with exotic properties were proposed, such as Electromagnetic cloak [1–3], Electromagnetic wave absorbers [20–22], Terahertz electromagnetic metamaterials [23–25], etc.

Inspired by photonic crystals, Liu et al. [26] put forward locally resonant phononic crystals, which opened the prelude to the study of AMMs. With further research, AMMs with both negative equivalent modulus and equivalent density, the two most important parameters for acoustic materials, were realized by dispersing soft rubber in water [13]. That double negative AMMs could achieve a negative refractive index. It was widely accepted that acoustic MMs all relied on locally resonant units to realize their extraordinary properties [27] until Norris [28] proposed pentamode metamaterials (PMMs) with effective density and bulk modulus could be regulated in a large range without reso-

nant phenomenon. The mentioned PMMs had fluid properties and could decouple effective bulk modulus and density, meaning that the most important two parameters could be designed separately without affecting each other. Afterward, varieties of acoustic MMs, such as acoustic cloaking metamaterials (ACMs) [5,29–31], acoustic absorption metamaterials (AAMs) [32–35], acoustic focusing metamaterials (AFMs) [36–38], were proposed.

With further research of MMs, great progress has been made in the study of mechanical and thermal metamaterials. Auxetics referred to materials with negative Poisson’s ratio (NPR) [6,39] and was first introduced by Evans in 1991 [40], playing an important role in MMMs [41]. This phenomenon is mainly attributed to their unique microstructure and composites designs [40,42] and can improve mechanical properties such as enhanced shear moduli, indentation resistance, fracture toughness, and impact energy absorption, etc. [41]. The research of TMMs was mainly targeted at controlling the heat flux by carefully arranging the distribution of different materials and designing microstructures. Furthermore, the TMMs could be combined with other kinds of MMs to achieve multi-function.

The fantastic properties of MMs are mainly realized by designing the structure and combining various materials, the traditional processing methods, such as casting, welding, molding, etc., were time-and-labor-costing in fabricating them, and some sophisticated lattice structures even can not be manufactured.

**TABLE 1****Acronyms.**

Acronym	Meaning
AAMs	Acoustic absorption metamaterials
ACCs	Acoustic cloaking carpets
ACMs	Acoustic cloaking metamaterials
AFMs	Acoustic focusing metamaterials
ALs	Acoustic lenses
AM	Additive manufacturing
AMMs	Acoustic metamaterials
BCC	Body-centered cubic
CLIP	Continuous liquid interface production
CPS	Compliant porous structure
DLW	Direct laser writing
DMRs	Decorated membrane resonators
EM	Electromagnetic
EMMs	Electromagnetic metamaterials
FCC	Face-centered cubic
FDM	Fused deposition modeling
FEM	Finite element method
FIB	Focused Ion Beam
HMMs	Hyperbolic metamaterials
IR-SPRs	Infrared surface polariton resonances
MMMs	Mechanical metamaterials
MMs	Metamaterials
NPR	Negative Poisson's ratio
PCB	Printed circuit board
PCs	Photonic crystals
PDMS	Polydimethylsiloxane
PMMs	Pentamode metamaterials
SC	Simple-cubic
SLA	Stereolithography apparatus
SLM	Selective laser melting
SLS	Selective laser sintering
SRRs	Split-ring resonators
TMMs	Thermal metamaterials
TPMS	Triple periodic minimal surface
TPP	Two-photon polymerization

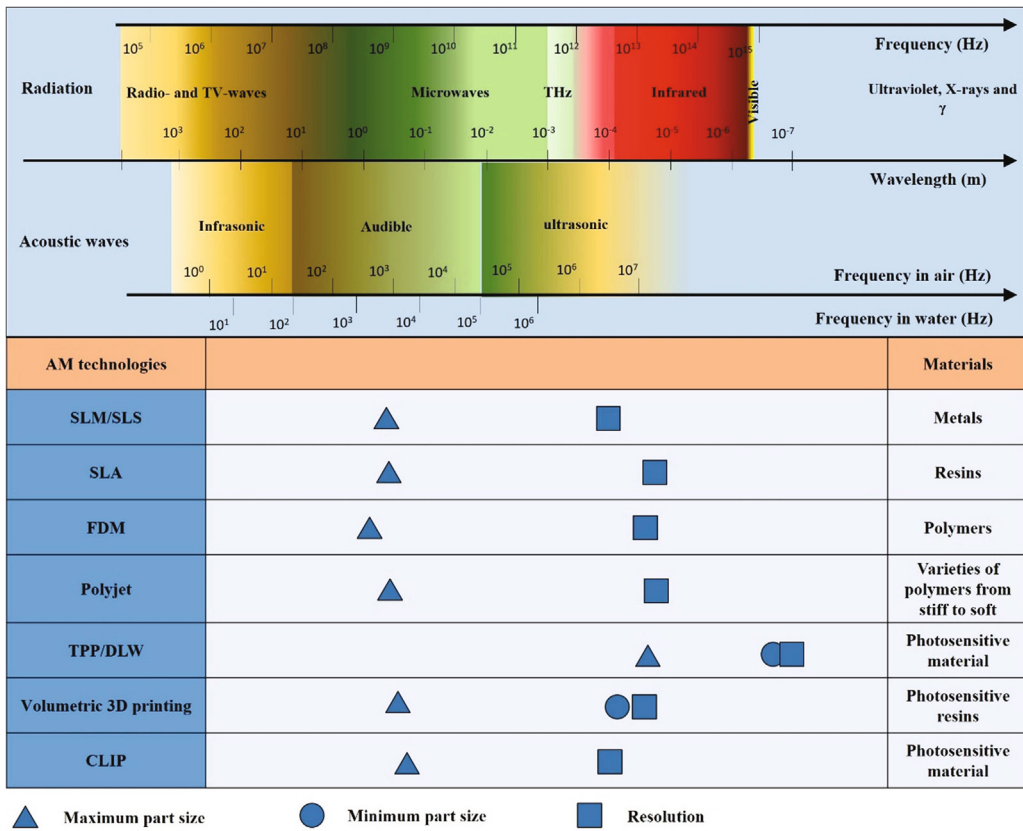
Thanks to the appearance of AM technology, the fabrication and experiment verification of MMs could be realized more conveniently and efficiently. By discretizing a 3D model of an object into several thin layers and accumulating them layer by layer,

the AM technology is capable of fabricating any complicated structures in theory. Besides, AM has been greatly enriched after nearly 40 years of development since it was patented in 1979, more than 20 AM technologies have been recognized [43]. Moreover, new technologies are still emerging [44–50]. For example, Daniel Oran et al. [47] proposed a nano-scale AM technology by volumetric deposition and controlled shrinkage, which could use more than one functional material at the same time. Moreover, materials with different properties, including metals, semiconductors, and biomolecules could be utilized.

On the whole, according to the forming material state, AM technologies could be divided into wire-based, liquid-based, powder-based, and mixed liquid-powder-based types. The applicable materials contain metals, polymers and ceramics [43], and the manufacturing dimension ranges from nano-scale [45,47,49,51–54] to meter-scale, which can greatly meet the ultra-high requirements of most MMs. Moreover, AM technologies could work by automatic control software and equipment, which greatly saves laborers. The examples of the applications of AM technologies in MMs were listed in Table 2. However, it should be noted that different AM technologies have different characteristics, such as the forming materials, size, resolution, and surface quality are all of significant difference. In the aspect of MMs manufacturing, it is necessary to select the appropriate technology according to the structure and the characteristics of the required material. Fig. 2 illustrated the manufacturing characteristics (mainly referred to manufacturing size and resolution) and applied materials of some typical AM technologies, which would reveal the limitations of AM technologies in fabricating MMs with various dimensions. Though the figure is mapped with the reference to acoustic and electromagnetic waves, it has general applicability in balancing the manufacturing resolution and size of MMs. It needs to be clear that although AM technology develops rapidly, there are still some limits at the aspect of manufacturing some types of MMs, such as ultra-fine nanoscale complex structures, multi-material systems, ultra-large structures, and so on. These problems will be discussed in detail in the text.

**TABLE 2****The examples of the applications of AM technologies in MMs.**

Types of MMs	Functionality	Materials	Dimension of the sample/mm	Types of AM technologies	Reference
EMMs	Electromagnetic cloak	Photoresist	0.09 × 0.09 × 0.01	DLW	[55]
		Photo-curable resin	246 × 100 × 6	SLA	[56]
	Millimeter-Wave waveguide	Cu-15Sn powder	3.10 × 3.10 × 1.5	SLM	[57]
	Electromagnetic absorption	Conductive ABS	300 × 300 × 6.5	FDM	[58]
AMMs	Acoustic absorption	ABS	49 × 25 × 80	FDM	[35]
		Polymer	2.3 × 2.3 × 10.6	[34]	
TMMs	Acoustic cloak	Plastics	–	SLA	[59]
	Ultralow thermal conductivity	Epoxy resin	–	SLA	[60]
	Improving thermal conductivity	Hexagonal boron nitride (hBN)/TPU	80 × 80 × 1	FDM	[61]
MMMs	Thermal camouflages	AlSi10Mg	6.4 × 16.8	SLM	[62]
	Elasto-mechanical unfeelability cloak	Polymer	1 × 1 × 2	DLW	[63]
	negative Poisson's ratio	ABS + maerials	50 × 50 × 5	Multi-material 3D printing	[64]
	Vanishing shear modulus	Ti6Al4V	34.64 × 60 × 10	SLM	[65]

**FIGURE 2**

The manufacturing characteristics and applied materials of some typical AM technologies. The triangle, circle and square represent the maximum part size, minimum part size, and manufacturing resolution, respectively. The position of the symbol represents the dimension corresponded to the wavelength. The distance between two symbols represents the achievable amount of unit cells per AM technology.

In this review, we will introduce the fundamental principles of different MMs and the typical types of MMs in various fields, as well as the applications of AM technologies in them. Furthermore, the limitations of the existed MMs and AM technologies will be concluded. We emphasize that AM technology is a suitable method for MMs fabrication and conversely the research of MMs could promote the development of AM technologies.

## The applications of additive manufacturing in metamaterials

### *Electromagnetic metamaterials*

Electromagnetic metamaterials (EMMs) are man-made composite materials/structures patterned on the sub-wavelength scale with periodic/quasi-periodic microstructures to achieve exotic electromagnetic properties not seen in natural materials. The response of materials to electromagnetic wave is usually characterized by two physical parameters, magnetic permeability  $\mu$  and electric permittivity  $\epsilon$ , which are both modulated by properties of parent materials, topological design and the spatial distribution of microstructures. Based on the equivalent electromagnetic characteristics of medium with different permeability and permittivity, the EMMs can be classified into normal materials, single-negative ( $\mu$ -negative or  $\epsilon$ -negative) materials, double-negative materials, zero refractive index materials (also called left-hand materials) [11,15]. The main traditional fabrication and implementation

methods of EMMs include photolithography [66], printed circuit board (PCB) processing [67], graphene-based materials [68,69], full dielectric resonance [70–74], stratified isotropic material combination [75], and photonic crystal [76]. The realization of EMMs based on PCB technology is to cover the metal materials on the dielectric substrate by means of printing or electroplating. The split-ring resonators (SRRs) that exhibit a series of negative  $\mu$  values made of nonmagnetic materials are typical electromagnetic components fabricated by PCB processing [12,77,78]. Graphene, a 2D material with the carbon atoms arrayed in vertexes of honeycomb lattice, represents unique optical transparency, flexibility, high electron mobility and conductivity, which can be tuned by electrochemical potential to realize the gate-controllable light matter interaction [79–81]. The results showed that the conductivity of zero doped graphene is independent of any material parameters, only a function of fine structure constant, but once doped, it has completely different performance, and its conductivity has changed greatly [68]. The bulk permittivity of graphene is determined by many parameters. Under the condition of fixed working frequency and temperature, it can be properly regulated by parameters such as chemical potential and damping coefficient. Most of the EMMs designs and fabrications were conducted with the use of metallic materials, in which the drawbacks consisted of conduction loss, fabrication difficulties and highly anisotropy composites, especially in the optical frequencies. When the transmission efficiency,

manufacturability from radio frequency to optics and isotropic design were considered, full dielectric resonance was recommended that can additively achieve wider bandwidth at the electric and magnetic eigenfrequencies due to the large fraction of volume and the occurrence of molecular resonances [70]. However, full dielectric metamaterials offer fewer freedoms of design because of weaker interacts under a given wave [82]. EMMs with required permittivity properties can be realized by a layered combined structure of thin alternating layers of metal and dielectrics, which have applications in many areas, including subwavelength imaging, negative refraction, optical hyper lenses and invisibility cloaking [75]. SRRs' feature size is only dozens of microns or 0.05% of the operating microwave wavelength, so that the structure appears to be uniform with minimal effective conductivity. However, limits of manufacturing technology, design options and consequently the intense sensitivity of perturbations and the above mentioned material loss probably hinder the realization of EMMs in the practice. Photonic crystal (PC) structures that may be used to achieve unprecedented electromagnetic performance, such as approximate cloaking effect, were proposed [76]. PCs are materials in which the refractive index varies periodically in different dimensions. The spatially varied refractive index in a PC determines the existence and properties of the optical equivalent and the photonic bandgap [83].

Furthermore, according to the application frequency, these EMMs can be divided into microwave, radio-frequency and terahertz types. The dimension of microwave and radio-frequency metamaterials is millimeter-level while the terahertz metamaterials should be fabricated with the characteristic size of microstructures below several tens of micron order and even in nanometer featured size, which is challenging for the conventional fabrication methods. Although nanopatterning methods such as lithography could be used for the fabrication of EMMs, such small-scale manufacturing techniques lead to the limitation of a wide variety of applications of metamaterials.

Because of their extraordinary physical properties and flexible manipulation, EMMs have been paid close attention to since they came into the attention of researchers in the early 21st century, and have been rapidly applied in military industry, communications and biomedical fields, meanwhile achieved rapid development. Through ingenious engineering of their property, dispersion and anisotropy, many design options become possible, including electromagnetic cloak, electromagnetic wave absorbers and terahertz electromagnetic metamaterials and more. Here is a detailed discussion of these typical applications of EMMs as following.

#### *Electromagnetic cloak*

Invisibility cloak made by EMMs is theoretically based on the transformation optics approach controlling the light propagation path through establishing a correspondence between material constitutive parameters and coordinate transformations [2,84,85]. Such a technique of transformation optics enabled to design conceived optical components that can modulate the EM waves with high degrees of freedom, resulting in many interesting functions, in which the invisibility cloaking in different frequencies ranging from electronics to optics is perhaps the

most famous and intriguing (Fig. 3). Prior to the realization of the practical EM cloak, the EM cloak was theoretical until the emergence of metamaterials. The first experimental demonstration of EM cloak using transformation optics was realized at a microwave frequency by constructing SRRs to obtain gradient permeability in planar space [1]. Besides, scattering cancelation [2,3] and quasi-conformal mapping [86,87] have also been developed to design EM stealth devices. However, the magnetic resonators, acting as a pivotal component to achieve cloaking effect, are often bulkier and thicker than the hidden object due to the difficulty to be miniaturized inside the optical frequency regime, otherwise leading to the high loss and kinetic inductance of electrons [88]. To overcome the barrier of the complexity of materials and bulky metamaterials, the recently proposed metasurfaces can control the wavefront optionally through introducing abrupt phase changes [89,90], in which the carpet cloak is the representative stealth device of metasurfaces derived from the quasi-conformal mapping theory [86] and PCs [55,56]. Moreover, compared to severe loss and bandwidth limitation of resonant metamaterials [56], the carpet cloak only requires a gradient refractive index in isotropic dielectric materials, and thus possesses low-loss and broadband operations. Using an artificial EM surface to build a carpet structure, when the EM wave is incident from the top of the head, it can insure that the reflected wave returns along the original path, just like the effect of EM wave on a flat plate. To achieve this goal, the reflection phase of the artificial EM microstructures on the surface needs to be adjusted. In order to compensate for the optical path difference of the EM beam corresponding to the adjacent microstructure, the phase between the adjacent microstructures needs to be changed [91,92].

Due to the current design approaches, most metasurface cloaks are considered as a 2D version of metamaterials and intensely dependent on a collective response. Based on a point-by-point wave reconstruction, the EM cloaking applied to an arbitrarily shaped object on a surface was developed, and further demonstrated successful concealment of electrically both large 2D and 3D structures at optical wavelengths [92]. Besides, a thin dielectric metasurface was used to reshape the wavefronts distorted by a scatterer, which can effectively make the stealth device work in a higher frequency band [93]. In terms of fabrication of carpet metasurfaces, a silicon-on-insulator wafer was firstly fabricated where the top silicon (Si) served as a 2D waveguide by using Focused Ion Beam milling (FIB) [87]. The experimental demonstration of optical cloaking with a curved reflecting surface to avert sharp transition and accordingly weakness of the cloaking performance that often happened in two planar metasurfaces assembled manually into a triangular shape [94]. However, a nonplanar substrate of metasurfaces fabricated by traditional manufacturing techniques, such as FIB, PCB, is difficult and costly for current machines and technologies. Recently, 3D printing technology has provided an opportunity to fabricate arbitrarily complex structures with high efficiency and precision. A carpet cloaking designed by gradient index PCs based on transformations optics and quasi-conformal mapping could be manufactured with smooth continuous graded microstructures by stereolithography with photo-curable resin [56]. Such EM carpet cloaking constructed by gradually altering

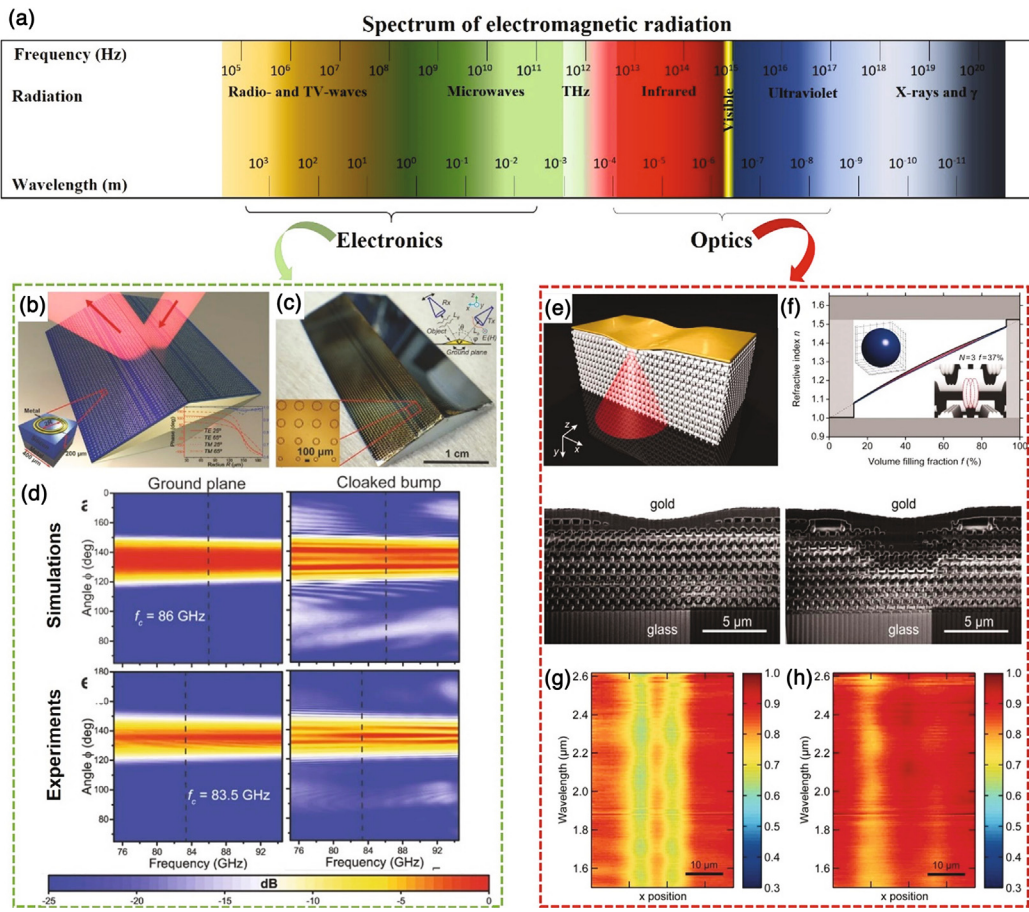


FIGURE 3

Realizations of EM cloak in different frequency from (b-d) electronics [94] to (e-h) optics [55]. (a) A spectrum of electromagnetic radiation. (b) Schematic illustration and (c) photographs of the fabricated metasurface EM cloak. (d) The radiation pattern for a ground plane and cloaked bump at the optimum incidence angle  $\theta = 45^\circ$ . (e) Blueprint of 3D carpet-cloak structure. (f) The local polymer volume filling fraction in the function of the effective local refractive index, oblique-view electron micrographs of fabricated structures after FIB milling, a bump (e) without a cloak and (f) with a cloak, the image intensity is shown on a false-color scale. (g) Without a cloak and (h) with a cloak.

the microstructure constitutive parameters of diamond lattices with orthogonal isotropy properties can realize the required spatial redistribution of the refractive index profile to reduce the scattering of the EM wave. Besides, 3D invisibility cloaking structures using tailored, dielectric face-centered-cubic (FCC) diamond-symmetry woodpile photonic crystals could be achieved in practice by direct laser writing (DLW) lithography instrument [55].

However, the prominent advantage of EM carpet cloaking is its ultra-thin characteristics, and the biggest disadvantage is its directionality, that is, it can only achieve EM invisibility for EM waves in a specific incident direction. When the incident direction changes, the stealth effect decreases significantly. With the development of 3D printing technology for smart materials [44,45,95], it is possible to realize a dynamic and controllable EM microstructure and a new type of stealth device that can dynamically adjust the phase distribution according to the incident direction.

#### Electromagnetic wave absorber

The conception of EM wave absorber proved significantly serviceable for modern science and engineering, nevertheless few

of the natural materials come close to 100% absorption for all angles in a broad bandwidth. The emergence of metamaterials makes it possible to design and manufacture EM wave absorbers. The artificial EM absorber, also called EM black hole, has been achieved by using resonant and nonresonant metamaterial structures for transverse magnetic modes and transverse electric modes in the microwave frequencies, respectively [96].

Current techniques for designing and fabricating EM absorbers have enabled the realization of such functional devices from microwave to optical frequencies, as shown in Fig. 4. In microwave frequencies, an omnidirectional electromagnetic absorber has been realized based on the theoretical prediction using non-magnetic MMs [20]. When working at terahertz frequencies, a thermally tunable multiband metamaterial absorber comprising a periodic array of closed metallic square ring resonators and four metal bars parallel to the four sides of the square ring has been designed and exhibited [22]. For optical EM absorbers, an approach to broadband omnidirectional light absorber that was independent of a magnetic response was developed [97]. To meet the needs of multiple frequency bands, an EM absorber consisting of ten discrete layers of MMs was designed and could work over a moderate wideband range, suitable for both micro-

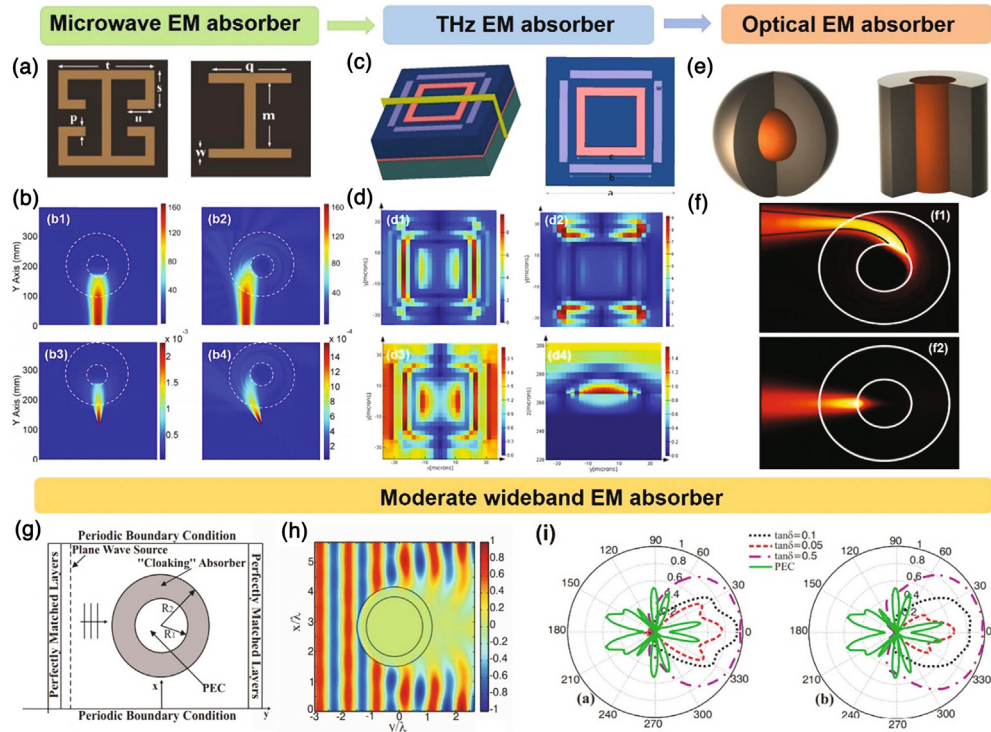


FIGURE 4

Design of EM absorbers for various electromagnetic fields. (a-b) Two kinds of unit cells of microwave EM absorber, and the full-wave simulation result under the (b1) on-center incidence, (b2) off-center incidence, (b3) vertical, (b4) oblique incidence [20]. (c and d) Architectures of THz EM absorber and distributions of the electric-field at different THz frequencies [22]; (e) The views of the spherical and cylindrical optical "black holes". (f) A Gaussian beam incident on the "black hole" off panel (f1) and on-center panel (f2) [97]. (g) Constructions of cloaking EM absorber. (h) Magnetic field. (i) Scattering coefficient pattern as a function of the loss tangent for the reduced "cloaking" absorber, and the ideal "cloaking" absorber [98].

wave and optical-based on several popular designs of electromagnetic cloaks [98].

Although it is possible to solve the limitation of the requirements of a specific range of incidence and narrow bandwidth, the designed transformation media are complex materials that are inhomogeneous and anisotropic, which lead to novel fabrication difficulty. Introducing a graded refractive index media operating in the homogenization regime can be a possible solution. For instance, an EM wave propagation of a 2D optical black hole with graded-index PCs was validated by the implementation of the proposed system in the metamaterials regime and then the optical properties of the designed device was confirmed by finite element method (FEM) [21]. Furthermore, the gradient index design strategy also acts on 3D EM absorbers. The 3D practical implementation of the optical black hole with the design of non-resonant gradient index PCs was fabricated by SL process. Absorbing ability at omnidirectional EM wave of the device in a broad bandwidth (12 GHz-15 GHz) were validated by full-wave simulation and experiments [99].

MM is prospective for the development of thin thickness and high-efficiency EM wave absorber, however, effective absorption can be achieved only in the resonance frequency band [100,101]. Adding multiple frequencies selected surface or multiple resonance structures is a valid method to broaden the bandwidth of traditional 2D MMs. However, the complex manufacturing processes confine their further applications. 3D MMs can also greatly enhance the EM attenuation capacity and broaden effec-

tive bandwidth by the synergistic action of microscopic and macroscopic effects [58,102]. Jiang et al. [102] designed a 3D honeycomb structure absorber with an absorptivity of more than 90% in a 3.53–24 GHz frequency band. Chen et al. [58] achieved an absorption coefficient absorption more than 90% within the frequency range from 5.3 to 18 GHz by an 3D printed sample. The current problem of fabrication techniques is that the resonant frequency shift and the diffuse reflection could be formed by the little manufacturing inaccuracy of the surface roughness, respectively.

For the EMMs with nanometer featured size, microscale AM thus holds great potential. Yoon et al [52] drastically increased the overlay accuracy of sub-20 nm based on carefully designed align marks and calibrators. And the fabrication of 3D suspended, interlayered and hierarchical nanostructures by accuracy-improved electron beam lithography overlay was completed. Furthermore, different from traditional 3D printing that adopts a layer-by-layer fabrication process, a type of 3D printing called volumetric AM uses light to rapidly solidify an object in a volume of a liquid precursor, which would significantly enhance the printing efficiency [48]. For its high-resolution 3D printing in seconds, the technology also could be a candidate for the realization of EMMs.

#### Terahertz electromagnetic metamaterials

Terahertz wave refers to the electromagnetic wave with the frequency ranging from 0.1 to 10 THz and the corresponding

wavelength ranging from 0.03 to 3.00 mm, between microwave and infrared. Application of terahertz radiation is paving a new era in a wide range of fields, particularly contactless imaging, biological nondestructive testing, time-resolved spectrum, extraction of optical parameters, material identification and high data rate communication, which are attributed to the natural characteristics of high transmissivity, low energy, transient, coherence, fingerprint spectrum and high bandwidth [24,25,103–106], as shown in Fig. 5. Metamaterials have been considered a promising route to construct terahertz devices, which can effectively manipulate both electromagnetic properties of a medium by designing 3D resonating elements. The only problem of these terahertz EMMs is that the devices with complex geometry and composition are difficult to be fabricated. Besides, owing to the fact that natural materials have weak wave–matter interaction at terahertz frequencies, the choice and availability of dielectric materials that provide adequate interaction while retaining the efficiency of the device has proved challenging [23].

In the term of fabrication, terahertz components and devices are mainly manufactured by cleanroom microfabrication facilities in the past decades. For moving away from less profitable high-end applications, engineered manufacturing is forced to create a new technology that can provide inexpensive and efficient terahertz components. Thanks to the uninterrupted innovation of materials and processes in the 3D printing industry, different types of terahertz devices have been designed, fabricated and experimentally verified, with even enhancing performances. For instance, a waveguide and a horn antenna were designed and fabricated by SLA-based manufacturing process for mm-wave applications, and these devices exhibited inferior transmission losses and matched closely a metallic split-block reference antenna in terms of cross-polarization and directivity [107]. SLM and DLW techniques have been applied to the manufacturing of metallic rectangular waveguides. A rectangular Cu–15Sn waveguide for mm-wave was fabricated by SLM, showing

process simplicity and mechanical robustness [57]. The attenuation of SLM-built waveguides is comparable with nonmetallic and commercial ones. Except for metallic waveguides, all-dielectric waveguides and fibers have also been studied by AM technologies. An antireflection waveguide structure was manufactured by MultiJet Printing (material jetting) technology, presenting a low loss and close-to-zero dispersion characteristic ranging from 0.2 to 1.0 THz [108]. However, the occurrence of dimensional deviations of AM processes would lead to mismatch loss and dissipation loss. Therefore, the printing parameters should be adjusted to match the practical experience, and a post-processing procedure may be required to achieve a good processing quality.

#### *Acoustic metamaterials*

AMMs refer to artificial structures or composites, composed of identical or gradually changing elaborately designed cell arrays, which can manipulate sound waves within sub-wavelength scales. Through carefully designing the microstructure and dimension parameters of the AMMs cells, the two key physical parameters that are essential for the propagation of the sound wave in materials, effective density  $\rho$  and bulk modulus  $K$ , can be regulated in a large range, even to negative. Those characteristics can generate varieties of extraordinary properties such as low-frequency bandgap, negative index, acoustic cloaks, etc. The early AMMs samples were mainly fabricated by some traditional methods like machining and assembly. For example, by embedding the identical or gradually changing cylinder in air, liquid, or other elastic soft substance, a two-dimensional (2D) phononic crystal with acoustic wave focusing, negative parameters, or acoustic bandgap could be obtained [36,109–116]. However, sometimes the crystal lattice size is micron-order as the working frequency range of AMMs reaches a considerably high level, some micromanufacturing technologies such as laser processing, micromachining, chemical synthesis or corrosion, etc. were adopted to acquire a sample [117–121]. When it comes to complicated structures, the traditional methods suffer from great difficulties in fabrication, limiting the application of AMMs in a certain way. Fortunately, the emergence of AM technology offers an optimized solution for fabricating the 3D AMMs with complicated structures. For example, SLA was adopted to fabricate a phononic crystal while the two key parameters of which could be manipulated by the external magnetic field [122]. Such a type of metamaterials that could react to external stimulations was also called active metamaterials. In this part, kinds of AMMs and the application of AM in them will be introduced, moreover, the limitations and the challenges of AM technologies will be discussed in detail.

#### *Acoustic cloaking metamaterials*

Inspired by the EM cloak, the ACMs were firstly theoretically confirmed through analyzing the transformation-type solution for the 2D acoustic equation [5]. The research showed that a shell with a gradient bulk modulus and mass density, designed based on the cloaking solution, was capable of controlling the scattering of the compressional acoustic wave so that the wave would bypass the shell without scattering, thus an ACM is achieved, as shown in Fig. 6(a). Followed by that, the theory of ACMs

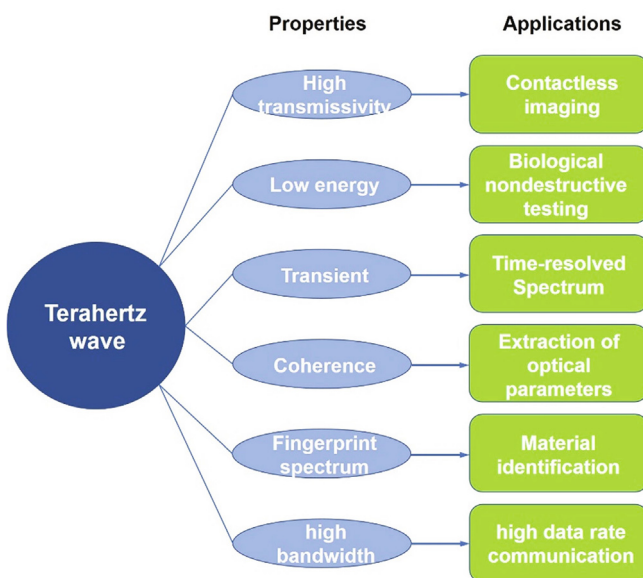
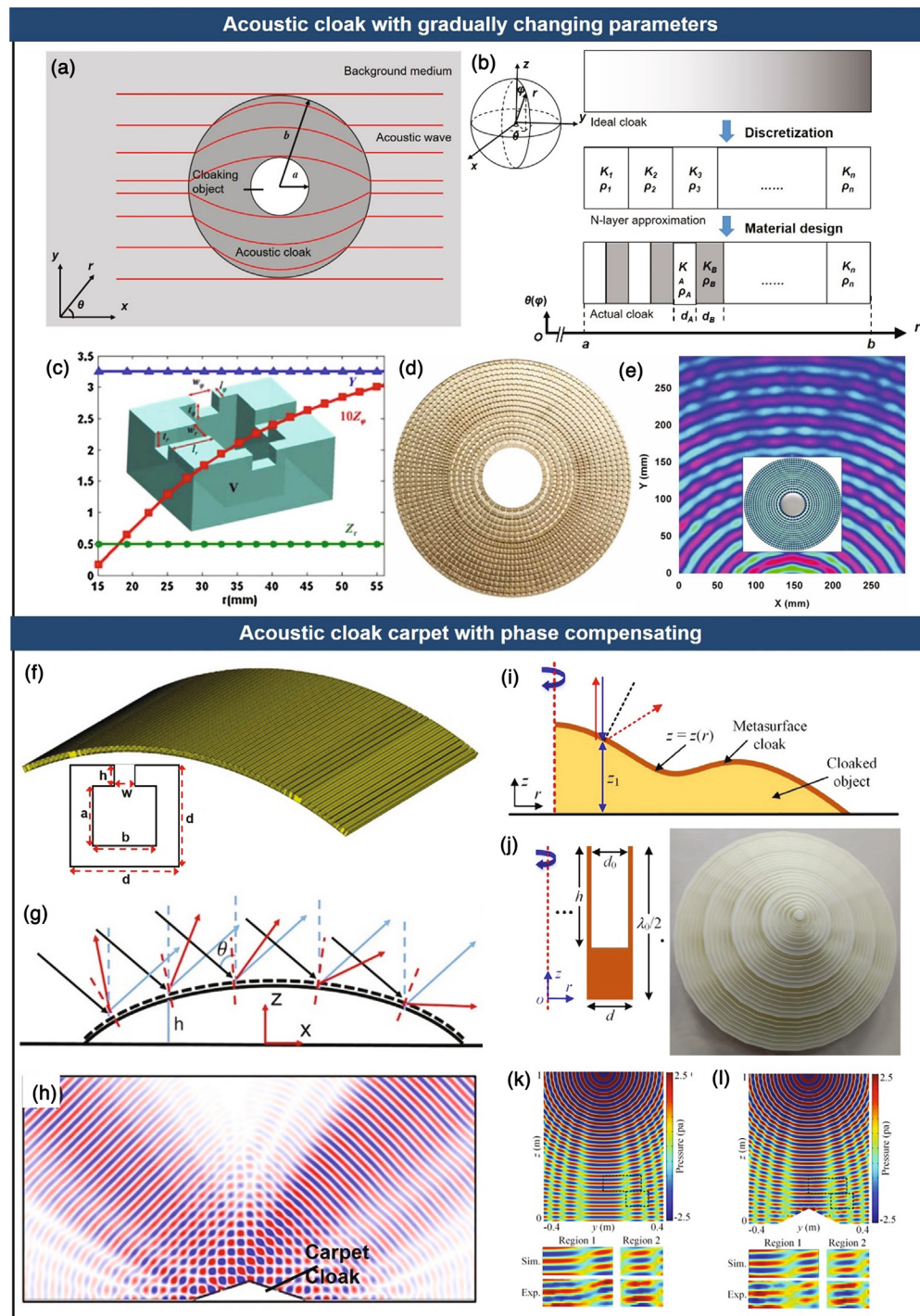


FIGURE 5

The properties and corresponding applications of the terahertz wave.

**FIGURE 6**

(a) The schematic diagram of the wave path through an AC. (b) design procedure of the multilayered cloak. [128]. (c) The conFiguration of the acoustic cylindrical cloak synthesized by an acoustic transmission line, namely, serial inductors and shunt capacitors. (d) The 2D AC based on acoustic circuit network. (e) Measured pressure field mappings of the AC at 60 kHz [29]. (f)–(h) The 2D acoustic carpet cloak [133]. (f) Perspective view of a metasurface skin carpet cloak. The inset picture is a typical unit cell of the metasurface cloak. (g) Scheme of a metasurface carpet cloak. (h) Pressure field distributions when an acoustic Gaussian beam is an incident onto cloaked bump from top left with an incidence angle of 45°. (i)–(l) The 3D acoustic carpet cloak [59]. (i) 2D cross-sectional illustration of an ACC with arbitrary shape. (j) Cross-sectional illustration of the basic groove structure unit (left) of the and the sample of the ACC fabricated by 3D printing (right). (k)–(l) Simulated and experimental total field distributions in the measured region 1 (left panels) and region 2 (right panels) for a spherical acoustic wave impinging on the flat ground and the object with the cloak.

was further supplemented [4,28,123–127]. The effective bulk modulus and mass density are expressed in spherical coordinate as below [127]:

$$\frac{\rho_r}{\rho_0} = \frac{b-a}{b} \frac{r'^2}{(r'-a)^2} \quad (1a)$$

$$\frac{\rho_\theta}{\rho_0} = \frac{\rho_\phi}{\rho_0} = \frac{b-a}{b} \quad (1b)$$

$$\frac{K_0}{K} = \frac{b^3}{(b-a)^3} \frac{(r'-a)^2}{r'^2} \quad (1c)$$

where  $\rho_0$  and  $K_0$  are mass density and bulk modulus of the background medium,  $\rho_\theta$  is the radial (normal to the interfaces) component of the effective anisotropic density tensors,  $\rho_\theta$  and  $\rho_\phi$  are the tangential (parallel to the interfaces) components of the effective mass density,  $K$  is the effective bulk modulus,  $a$  and  $b$  are the inner radius and the outer radius of the spherical shell respectively, and  $r'=a+r(b-a)/b$ .

The ACMs described by Eq (1) performed perfectly on the simulation verification [5,127]. As for acquiring a device, the key point is how to get a type of material with such distributed parameters as depicted by Eq (1). Obviously, such a material can not be found in nature. There were mainly two solutions to obtain an ACM sample.

One is to discretize the continuous distribution of physical parameters so that each discrete parameter can be replaced by a certain material in nature, which provides a possible scheme for the realization of ACMs [29,111,123,124,126,128–130]. At first, supposed that there is a spherical shell with the bulk modulus and mass density distributed as Eq. (1). Then the parameters along the radius direction were discretized while the tangential direction is homogeneous, as shown in Fig. 6(b). The simulation results show that the AC will perform better when the layer number gets larger and the layer thickness is small enough compare to the acoustic wavelength [111,131]. However, though it seems that the aforementioned multi-layered ACMs are feasible to be fabricated, and a few researchers even have provided a certain material to get an AC sample [124,132], the evidence of experimental verification is still not found.

The main problem is that no materials can meet the properties combination depicted by Eq (1). Supposed  $a$  is 1 m,  $b$  is 2 m, the density of water  $\rho_0$  and bulk modulus  $K_0$  is 1000 kg/m<sup>3</sup>, 2.19 GPa respectively. Then the radial density distribution is  $2[(1+r/2)^2/r^2]\rho_0$ , and the bulk modulus distribution is  $2[r^2/(1+r/2)^2]K_0$ . When  $r$  is 1 m, the density is 4500 kg/m<sup>3</sup> and the bulk modulus is 1.95 GPa; When  $r$  is 2 m, the density is 2000 kg/m<sup>3</sup> and the bulk modulus is 4.38 GPa. Although this analysis is based on concrete values, it has general adaptability. As a result, the key to multi-material manufacturing lies in the selection of materials with relatively high density and low bulk modulus. When a material with such a properties combination is developed, the rapidly developing multi-material AM technologies may meet the manufacturing requirements [44,95,134]. For example, the multi-material 3D printer developed by Stratasys could obtain the behavior of resins ranging from stiff to rubber-like [95].

Another method is to use gradient-varying microstructures to replace multilayer materials [29,135,136]. The equivalent parameters of the structure can meet the distribution as Eq. (1) depicted through careful designing. Fig. 6(c)–(e) showed an ACM example achieved by replacing multi-layers of materials with gradient-varying microstructures composed of annularly arranged cylinders whose spatial geometry was carefully tailored. The cloak was fabricated by machining an aluminum plate into 16-step

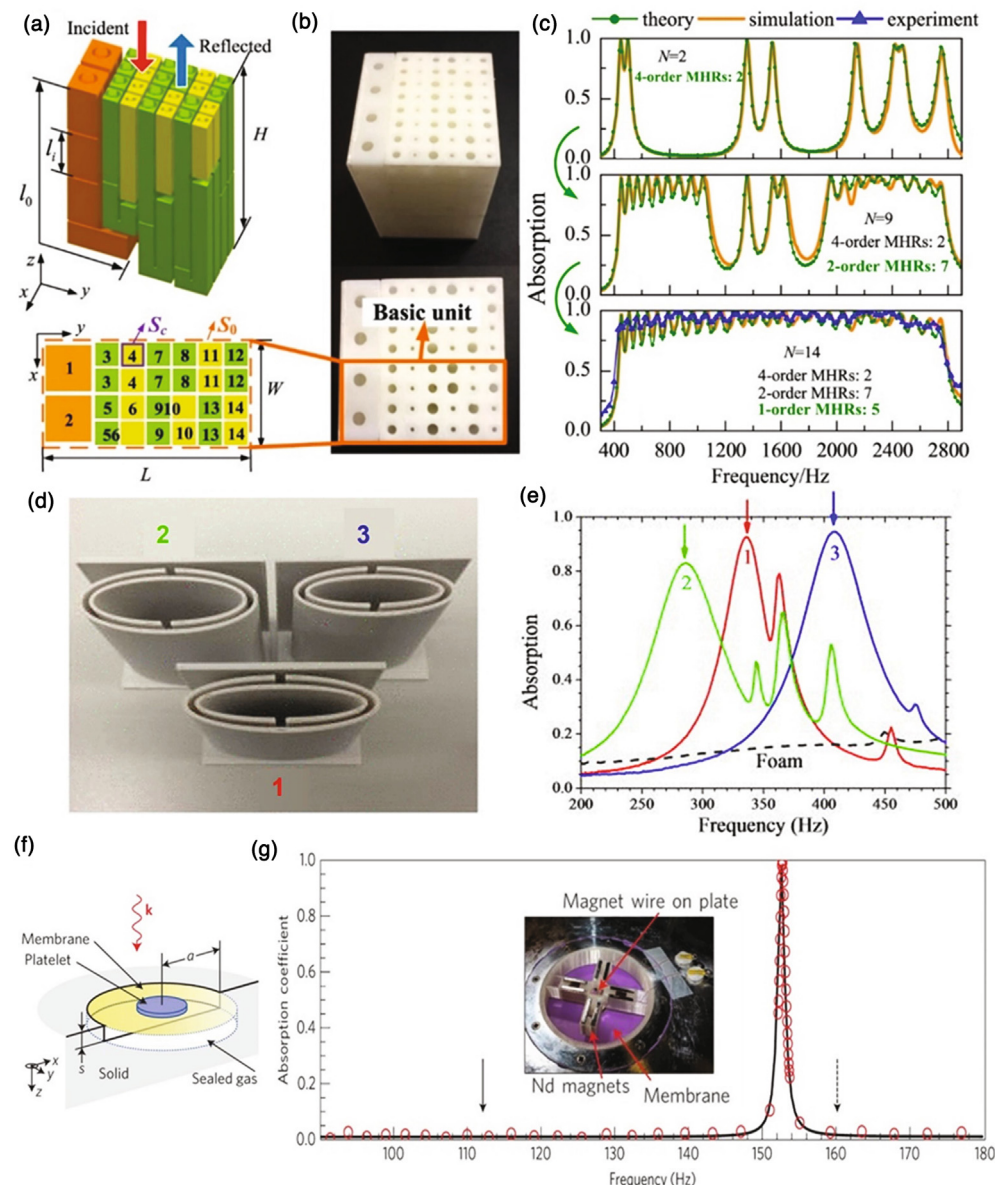
piecewise homogenous cylinders, as shown in Fig. 6(d). In fact, for such structures, some metal AM technologies, such as SLM, can provide sufficient accuracy, which is a more convenient and direct manufacturing method. However, few examples of the application of SLM in ACMs were found, which may result from its high cost, especially in large sample manufacturing.

With the further development of ACMs, the proposal of the acoustic cloaking carpet (ACC) provides a new way to realize acoustic invisibility [31,59,133,137–142]. In general, the 2D ACC is shaped like a carpet [133,142], on the surface of which a series of well-designed microstructures that could compensate for the phase distortion caused by the geometry of the cloaking carpet are imposed. Consequently, when the acoustic waves propagate to the cloaking carpet from a certain direction, the reflection orientation of the waves that should have been scattered becomes consistent (as shown in Fig. 6(g)), just like a mirror. The 3D ACC is mostly cone-shaped [31,59,138], Fig. 6(j) provides a typical model. The ACMs described by this theory mainly rely on the structure without any special requirement for raw materials. Moreover, there's no demanding requirement for the manufacturing accuracy due to the working frequencies of ACMs are mostly in the low-middle frequency range. Some economical and commercialized polymer AM technologies, such as FDM, SLA, selective laser sintering (SLS), etc., would achieve a good manufacturing effect. Fig. 6(j) showed an ACC sample fabricated by AM using polymers, and the simulation and experimental results (Fig. 6(k)–(l)) showed that it can work effectively within the range of 6200–7500 Hz [59].

On the whole, the ACMs could be achieved from two strategies. One is to control the acoustic wave through the gradient change of physical parameters. Obviously, it is a more general acoustic stealth theory, which can make the protected object resist the detection of broadband sound waves from all directions. However, as in the previous analysis, the main problem is to select appropriate materials to meet the matching of equivalent density and bulk modulus, and the interface connection of multi-material should also be considered. Another method is structural designing, which can solve the coupling of density and bulk modulus and can easily be fabricated by AM technologies. However, the main problem is that the structural design still stays at the 2D level.

#### Acoustic absorber

The research of acoustic absorption metamaterials (AAMs) is mainly targeted at the low-frequency region for its negative effect on human health. As the research shows, long-term exposure to a low-frequency noise environment will cause the body's brain central function to decline, prone to dizziness, and other diseases [283]. The sound transmission loss follows by mass density law [143], which reveals that the greater areal mass density is necessary to block out the low-frequency noise, which makes it difficult for practical application. Traditional sound absorption material, such as porous material, has great performance at relatively high frequency for the inner void can provide a greater acoustic energy attenuation coefficient, making sound waves dissipate faster. However, when it comes to low frequency, it suffers from great difficulty. Therefore, it is a challenging task to control the propagation of low-frequency sound waves within

**FIGURE 7**

Different types of AAMs. (a)–(c) Multi-order Helmholtz resonators: (a) Basic unit of the MM composed of  $n$  coiled MHR cells. (b) Photograph of the sample fabricated by 3D printing. (c) The process to critically couple the cells of the MM with broadband absorption and the comparison of the results between theory, simulation and experiment [35]. (d) and (e) Split tube resonators: (d) Photograph of three samples fabricated by 3D printing. (e) Measured absorptions of the three samples [151]. (f)–(g) Decorated membrane resonator: Geometry and resonance characteristics of the metasurface's unit cell and its absorption spectrum: (f) Schematic illustration of the unit cell's components and geometry. (g) Measured sample (insert picture) and absorption coefficient as a function of frequency [154].

reasonable size, and the proposal of AAMs provides a new solution. For an acoustic absorber, its acoustic absorption coefficient can be expressed as:

$$\alpha = \frac{4x_t}{(1+x_t)^2 + y_t^2} \quad (2)$$

where  $\alpha$  is the sound absorption coefficient,  $x_t$  and  $y_t$  are the acoustic resistance ratio and acoustic reactance ratio compared to the background acoustic characteristic impedance respectively. It shows that when the acoustic resistance ratio is 0 and the sound resistance ratio is 1, the sound absorption coefficient of the AAMs will reach 100%.

Most of the AAMs are based on the local resonance effect. One of the important contents of AAMs is derived from micro-perforated plates, composed of two major components, the micro-perforated plate, and the back cavity. The micro-perforated plate provides an acoustic resistance and reactance, and the back cavity is equivalent to an acoustic reactance. The value mainly relies on the dimension parameters of the structure and the physical parameters of the air. As it reaches the resonance frequency, the absorption coefficient reaches the maximum.

The back cavity of a traditional microperforated acoustic absorber is usually a straight channel. Large size of AAMs is

needed to achieve perfect sound absorption when the working frequency is very low, which makes it not conducive to practical application. To reduce the dimension of the absorber while ensuring its absorption performance, the coiled-up space was proposed, which could significantly reduce the size of the absorber [32,144–150].

Another type of AMMs is split tube resonator [151–153], consisting of channel, core and rigid backing, which derives from the EMMs [18]. As shown in Fig. 7(d), the whole structure is similar to a Helmholtz resonator, with the channel equivalent to a neck and the core equivalent to a cavity. Differently, the long and narrow channels will increase the viscous loss. When the incident wave reaches the resonant frequency of the structure, almost 100% sound absorption effect will be achieved.

The function of acoustic absorption of this type of AAM is completely caused by the structure, which is similar to the ACM. Therefore, just like the ACCs, some economical and commercialized AM technologies, such as FDM, SLA, SLS, etc., could meet the requirements. As shown in Fig. 7 (b) and (d), Multi-order Helmholtz resonators and split tube resonators were fabricated by SLA and FDM respectively, and the experimental and simulation results corresponded well (Fig. 7(c) and (e)).

Apart from the microperforated AAMs, the decorated membrane resonator (DMR), consisting of three major parts, membrane, platelet, and the back cavity, could also get a resemble acoustic absorption performance [33,145,154]. Fig. 7 (f) provides a schematic illustration of the DMR, the platelet was embedded into the middle of the membrane and the back cavity was sealed between the membrane and the solid substrate. The resonant frequency is mainly related to the mass of the platelet, the elastic modulus of the membrane, and the depth of the back cavity. The DMR will achieve a perfect absorption effect as the hybrid resonance takes place. As for fabrication, the AAMs mentioned in this part require a combination of stiff and soft materials, without the coupling of different physical parameters at the same time, which makes it easier to fabricate such an AAM by multi-material AM technology. For example, the multi-material 3D printer developed by Stratasys, as mentioned in section 2.2.1, may be competent for this work.

In general, the AAMs can achieve a perfect absorption effect within a certain frequency range while the bandwidth is quite narrow. Therefore, researchers have tried a lot to broaden the absorption bandwidth while the dimension parameter remains at the same scale [35,155,156]. Xue et al. [155] proposed broadband and robust AAMs that are composed of gradient arrayed rectangular sawteeth. The gap between two adjacent sawteeth is equivalent to a short tube. For the tubes with different depths can match different acoustic wavelengths to form a standing wave, the broadband sound absorption with the range of 1000~6000 Hz was realized, and the results were verified by the FDM sample. What's more, the acoustic absorption devices based on this type were even commercialized and could reduce noise by 7–9 dB within a frequency range of 400–2000 Hz [157,158].

On the whole, most of the sound absorption effect depends on the structure, and the requirements for materials are not demanding, so polymers could meet the needs. Moreover, the working frequencies of AAMs usually locate at the audible range, thus some conventional polymers AM technologies, such as

FDM, SLA, SLS, etc., are competent. However, there remains a small problem that the support of some complicated structures is needed but difficult to remove. If a better water-soluble support material is available, that is, it can dissolve, remove more quickly, and have no residue, it will greatly promote the fabrication of large-scale MMs devices with high precision and complexity. Besides, for the AAMs composed of multiple materials, such as DMRs, AM technologies still face some challenges, that is, how to combine materials with quite different properties firmly and achieve a wide range of parameters adjustment.

#### *Acoustic focusing metamaterials*

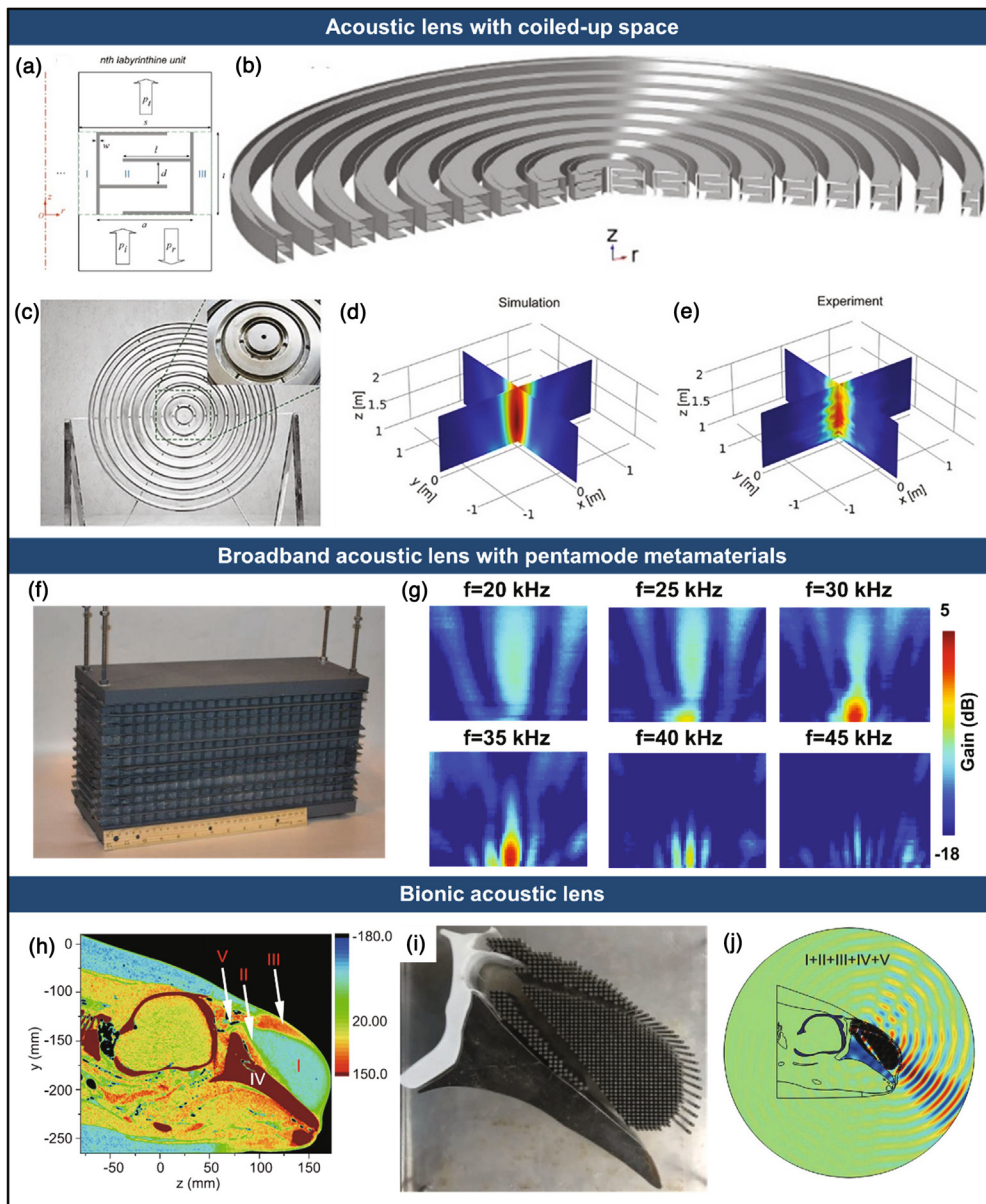
The effect of acoustic focusing could be achieved through two methods, reflective focusing and refractive focusing, which is similar to that of electromagnetic. The present research of acoustic focusing is mainly focused on the method of refraction, that is, acoustic lens (AL). There are two ways to achieve an AL, one is to obtain negative refractive index MMs by elaborately designed structures and the other is to mimic a biosonar. The artificial metamaterials usually obey generalized Snell's law [159]:

$$n_2 \sin\theta_t - n_1 \sin\theta_i = \frac{\lambda_0}{2\pi} \frac{d(x)}{dx} \quad (4)$$

where  $n_1$  and  $n_2$  are the refractive indexes of medium 1 and 2 compared to that of the air respectively,  $\theta_i$  and  $\theta_t$  are the incident and the refractive angle at the interface respectively,  $d\Phi(x)/dx$  is the accumulative phase change rate at the interface with coordinate, that is the change rate of the sonic path. The law shows that the acoustic waves can be manipulated by modulating the accumulative phase change rate  $d\Phi(x)/dx$ . The accumulative phase will be ascertained as the interface microstructure is determined, which makes it practicable for the realization of the accumulative phase gradient by gradient-varying interface microstructures. Actually, the theory can be used not only to design AL but also to achieve other regulation of acoustic waves, such as changing the propagation direction.

Based on generalized Snell's law, to obtain the accumulative phase gradient, varieties of microstructures are proposed to further realize the acoustic focusing effect. The microstructures design based on coiled-up space has achieved a great performance [32,116,160–166]. Unlike the AAMs, the coiled-up space used in ALs has two open ends, which can significantly delay the phase of sound propagation in a limited space. By changing the dimension parameters of the coiled-up space and combining them in a certain rule, a 3D AL was obtained and the experimental results are in good agreement with the simulation [116]. Each microstructure unit is made of steel and fabricated by machining in the reference and all units are assembled by two supporting shells (Fig. 8 (c)). Obviously, such a method needs a complex processing procedure and is time-consuming, AM technologies like SLM are the more ideal way. Like the AAMs mentioned in section 2.2.2, this kind of AL is completely structural dependent, and its working frequency range does not require very high forming resolution. Therefore, it is believed that it can achieve a good focusing effect via polymer AM technologies.

However, when the acoustic frequency deviates from the design frequency, a serious impedance mismatch between the AL and the background medium will appear, thus most of the

**FIGURE 8**

(a) Cross-section diagram of a unit of the proposed lens. (b) The schematic diagram of the three-dimensional axisymmetric acoustic GRIN lens. (c) The sample of the 3D-designed AL. (d) The simulated spatial distributions of the intensity field  $|p|^2$  of the AL. (e) The measured spatial distributions of the intensity field  $|p|^2$  of the fabricated sample [116]. (f) Photograph of the assembled lens. (g) The plots of the gain (dB) were exhibited due to the inclusion of the GRIN Lens [167]. (h) CT image of a neonate finless porpoise's head, where I, II, III, IV, and V correspond to melon, muscle, connective tissue, skull, and air sacs, respectively. (i) A sample of the physical-based porpoise model. (j) Experimentally measured and numerically simulated pressure distributions with a physical-based porpoise model. [168].

energy will be reflected, leading to the failure of achieving the expected acoustic focusing effect. One of the most important prerequisites for realizing a broadband acoustic lens is impedance matching. The acoustic lens based on the pentamode metamaterials (PMM) is an ideal choice to solve such a problem [167,169–171]. Because that the PMM can decouple the bulk modulus  $K$  and the effective density  $\rho$ , that is to say, the bulk modulus can be adjusted in a wide range without changing the effective density. Therefore, the accumulative phase gradient of the acoustic lens based on the PMM can be adjusted under the condition of maintaining the impedance matching, so as to realize the broadband acoustic focusing. To obtain a broadband AL, Su

et al. [167] took the PMM with different dimension parameters and arranged them within the predetermined gradient. The experiment results suggested that the AL could achieve a good focusing effect within 25~35 kHz. In the aspect of manufacturing, SLM is a more optimal choice that can not only form complex lattice structures but also has good surface morphology.

In addition to the artificial microstructure, the bionic structure can also effectively improve the directivity of sound waves, especially the biosonar of dolphins [168,172–175]. The research suggested that the biosonar of dolphins consisting of three major parts, soft tissues, air sacs and skull [173]. The soft tissues possess a gradient acoustic velocity. The interface between the air sacs

and the tissues is regarded as a soft boundary, plays an important role in controlling the propagation of sound waves. The skull has a large impedance mismatch compared with surrounding tissues and plays an important role in regulating the direction of sound waves. The combination of the three will generate a biosonar with high directivity. Different parts were replaced by similar materials or structures [168]. The skull was replaced by stainless steel and the air sacs were replaced by 3D printed acrylic mold. The soft tissues were further subdivided into mellon, muscle and connective tissues and were replaced by steel-water and aluminum-water composites with different filling volume fraction, so that the sound velocity in the substitute was approximately equal to that of the counterparts of the biosonar. Then the substitutes were assembled to obtain a bionic AL. the results showed that both simulation and experimental verification have achieved good effect.

On the whole, AM technologies are not very common in the fabrication of AFMs, though they are more admirable compared to traditional manufacturing methods. They can not only simplify the manufacturing process but also save labor costs. For MMs that need metallic materials, such as pentamode materials, SLM is an ideal choice. It has a larger forming size while maintaining a relatively high resolution (the minimum fabrication size is about 0.2 mm). When the AFMs operate at higher frequencies (for example, reached 3 MHz, the working wavelength of a medical machine), the smaller unit size is needed accordingly, thus SLM cannot meet the demand. Some micro-scale AM technologies [47,52,53], such as shrinking volumetric deposition [47], could solve the problem. However, these usually need a more complicated procedure compared to traditional AM technologies. Two main factors hinder their applications. On the one hand, it will cost a lot in forming large-scale ALs or using those micro-scale AM technologies. On the other hand, The variety of materials available is limited.

### *Thermal metamaterials*

Heat loss is an inevitable thermodynamic phenomenon, and the method of thermal energy guidance gets a lot of attention [176]. There is some manipulation that has been raised to directly convert the waste heat to effective energy with an unavoidable defect of low conversion efficiencies [177], such as thermoelectric and thermomechanical methodologies [178]. Therefore, a more effective approach to the channel of re-direction thermal energy has been brought up by designed TMMs [179]. The special attributes of TMMs include re-direction thermal conductivity, tunable electro-thermal [180] and induced anisotropy [181]. Then the TMMs adjust thermal flux through thermal gradient ( $\nabla T_i$ ) with the Fourier law of heat conduction:  $q_i = -\kappa_{ij}\nabla_j T_i$ . TMMs applicate to thermal concentrators [182,183] (concentrate heat into a specific region), thermal rotators [182,184] (rotate the flow of heat), thermal cloaks [181,185–191] (let heat flow around an object, Fig. 9) and camouflage [192,193] (which are used to let the heat signature of object B as a substitute for that of object A).

### *The control of heat flux*

To gain better control of heat transfer in a solid medium, the concept of a MM with particular arrangement of materials or an engineered sub-structure was in a wide range of studies. The spread of

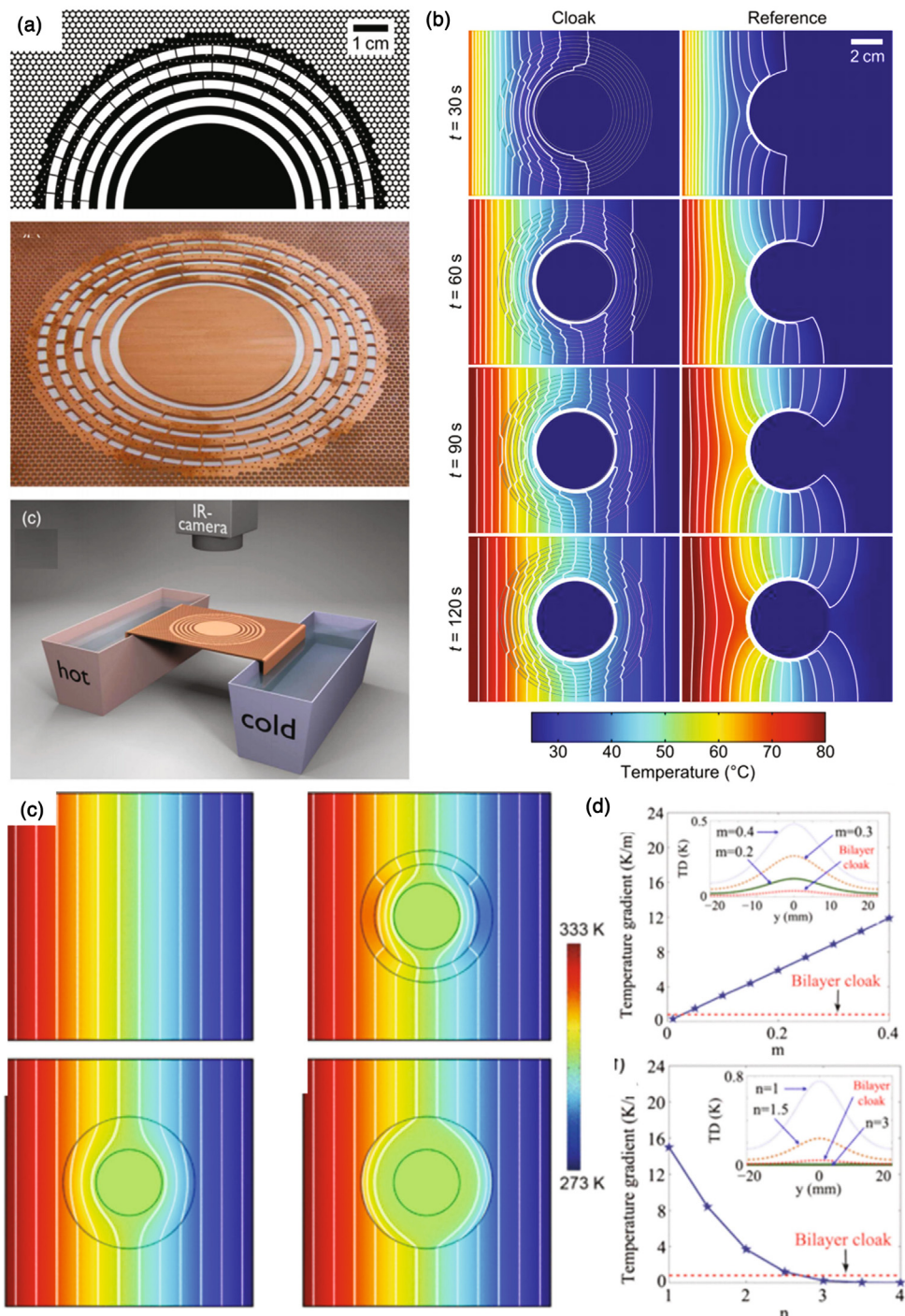
heat flux is controlled through the resourceful materials arrangement and the basic geometric criteria in the response of multi-layer composite materials. As similar to electromagnetic, the phenomenon that corresponds to positive or negative bending of the thermal flux generated by MMs, that contrived by stacking various materials with different nominally isotropic thermal conductivities. The control of heat flux is advantageous for controlling and guiding heat energy and reducing heat wastage [184].

In general, TMMs are prepared by the layering of isotropic or optimized arrangement [14,179]. The heat transfer can be significantly affected by the interfacial thickness and thermal conductivity for the case of diffusive transport. As a result, the influence of interface thickness and thermal conductivity on the heat flux through the composite medium by the method of a non-contact methodology using radiative imaging had been investigated. The result showed that a lower Al layer/silver interfacial epoxy ratio of ~25 could reduce the deviation of heat flux bending angle rather than that of an Al layer/alumina interfacial epoxy of ~39. Thus, the variation of interface parameters is critical to the heat flux variation in the composite and MM layers [194].

The research of TMMs by rational design and reasonable arrangement of materials is a benefit to the creation of elements aimed at channeling thermal energy, such as concentration or cloaking the heat flux. For example, the thermal extremum principle where the propagation of heat went through the path of least thermal resistance and the coordinate transformation was used to inducing anisotropy in thermal conductivity. When the direction of layers in the composite materials physically rotates relative to a constant temperature gradient, it would occur that thermal anisotropy due to a corresponding introduction of off-diagonal components induced in the thermal conductivity tensor [195]. The thermal concentration was implemented by alternating natural materials and the relation curves were obtained [186,187]. A TMM was designed by stack layers of stainless steel and copper, considering conductive heat flux and non-resonant structures in the effective thermal medium [176]. The result showed that they obtained an upward or downward heat flux bending of up to ±26 °C lay the foundation to design innovative thermal devices.

### *Thermal emission*

TMMs for engineering design of thermal radiation from the black body are expected to affect various applications including energy harvesting, thermal management, and coherent thermal sources. Because of surface electromagnetic excitations [197] or at the edge of bandgap in photonic crystals [198], there will be thermal emission beyond the limit of the black body, but the energy transfer only occurs in a narrow band. Guo et al. [199] overcame the limitations of super-Plankian thermal radiation at a single resonant frequency by used TMMs with engineered dielectric properties. Based on the singularity of the state bulk density of hyperbolic metamaterials (HMMs) [200], the unique property was the broad bandwidth between HMMs and conventional approaches of engineering the photonic density of states. To achieve the extreme anisotropy characteristic of HMMs, a metal-dielectric super-lattice structure which is phonon-polaritonic metal (silicon carbide SiC) was used. In this work, near field thermal emission was set up in a broad bandwidth

**FIGURE 9**

(a) The scheme of the designed thermal cloak. (b) Calculated temperature distributions shown as the experimental results [181]. (b) Temperature distributions and quantitative comparison for different thermal cloaking schemes: a pure background, bilayer thermal cloak, Al thermal cloak with  $m = 0.2$ , and AH thermal cloak with  $n = 3$ . (c) The tendency of the temperature gradient at  $(0,0)$  for the Al thermal cloak with different  $m$  and the AH thermal cloak with different  $n$  [185].

exceeding the black body limit from HMMs. They ascend as bulk high- $k$  propagating waves [200,201] in the MMs that cause a divergence of the density of states (effective medium limit) and lay the foundation for design near-field thermal engineering using HMMs.

It was demonstrated that radiative heat transfer can be tremendously increased through photon tunneling by evanes-

cent electromagnetic waves, while the band distance between objects is narrower than the prediction of dominant thermal wavelength by Wien's displacement law. When infrared surface polariton resonances (IR-SPRs) are supported by the interacting materials, near-field radiative thermal transfer gains several orders of magnitude over that predicted by Planck's law [202,203]. However, the near-field heat transfer based on

IR-SPR extremely depends on materials. It showed that heat transfer would be enhanced between two identical IR-SPR materials [204]. Contrarily, the surface polariton resonance supposed by different frequencies would strongly decrease near-field radiative heat transfer. It occurred due to the frequencies of the surface polariton resonances did not match when the absorber and emitter are made by two different materials. There is a design of IR-SPR with required frequencies by “MMs” put forward to break through the limitation of near-field materials [205]. Consequently, two conditions must be satisfied with MMs to maintain the effective characteristics of the design and control the heat radiation near-field: (i) the feature size of the MMs such as the period of subwavelength structures has to be narrower than the gap distance between the emitter and the absorber, which is within the scope of nanometers [206] and (ii) MMs have an effective resonant frequency in the infrared range such as wavelength around 10 μm. Therefore, a broadband nonresonant heat emitter/absorber has been come up that was based on hyperbolic MMs. And the near-field radiative heat transfer between IR-SPR thermal emitters and metals could be enhanced [205].

#### *Thermal cloak and thermal camouflage*

There are broader applications in thermal cloaking and illusion because that thermal camouflage can transform the actual perception into a pre-controlled perception as similar to wave-dynamic illusion [2,84,207,208]. The functional thermal camouflage device is capable of transforming the heat scattering characteristics of an object into the heat scattering characteristics of multiple isolated expected objects. It means that the device can equivalent the thermal scattering signature of the “cloaked” object to that of other multiple objects. The thermal camouflage device is based on the exact bilayer cloak fabricated only by natural materials, and it is designed without complicated MMs based on transformation optics suggested [209–213].

On the condition of time-dependent and thermal-dependent, it is the thermal camouflage with the exceptional thermodynamic performance that has been demonstrated. A functional thermal camouflage device that could create multiple prospected graphics off the primary object’s position in thermal conduction [192]. It showed that the thermal cloaking means an exposed “man” could be unambiguously detected from the thermal signature while the corresponding thermal signature vanished at the time that the “man” was covered by a thermal cloak. Furthermore, the thermal camouflage meant the thermal signature is extremely different from the former when the “man” shrouded by the designed device and is as same as that of the “man” pre-arrangement. Consequently, it can be realized through eliminate the thermal scattering of the original object with an exact bilayer cloak and succedent fabricated the thermal scattering signature by placing pre-designed and expected objects.

The thermal cloak could adjustment the inhomogeneity and anisotropy to tailor heat flux at will. As shown in Fig. 10, it has been demonstrated by experiment and simulation that the effectiveness of thermal cloak. The bilayer cloak is designed to have the outer layer of copper with a conductivity of  $\kappa_{Cu} = 394 \text{ W}\cdot\text{m}^{-1}\cdot\text{K}^{-1}$  and the inner layer of polydimethylsiloxane (PDMS) with a conductivity of  $\kappa_{PDMS} = 0.15 \text{ W}\cdot\text{m}^{-1}\cdot\text{K}^{-1}$  [181]. And the required

background conductivity can be realized by using PDMS to fill the holes drilled in the copper plate. And the PDMS area fraction  $f$  was calculated by the Maxwell-Garnett formula [214]

$$\kappa_b = \kappa_{Cu} \left[ 1 + \frac{2(\kappa_{PDMS} - \kappa_{Cu})f}{\kappa_{PDMS} + \kappa_{Cu} - (\kappa_{PDMS} - \kappa_{Cu})f} \right].$$

A cloaked copper object was transformed into two PDMS wing-ghosts in the thermal scattering signature in the thermal camouflage device by two expected objects set at the side of the bilayer cloak. Eventually, it was verified the function of thermal cloak and thermal camouflage by the finite element method and experiment, while the results of both were anastomotic [192].

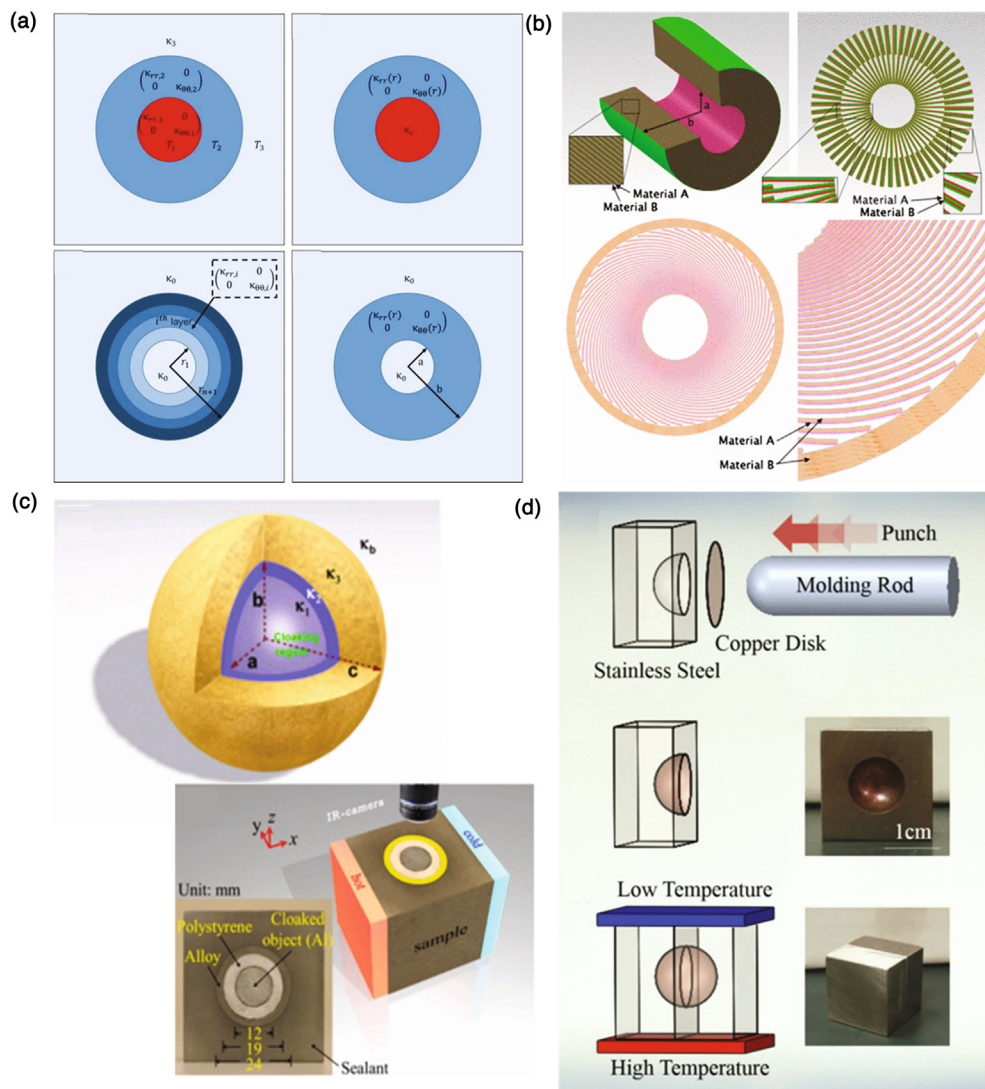
An effective method had been proposed to fabricate 3D omnidirectional cloaks with finite constant conductivity (without inhomogeneity and singularity). The cloak used periodically alternating isotropic conductivities instead of anisotropy. And the thermal localization inside the coating layer could be tuned by anisotropy. The method provided a reasonable approach for thermal cloak and manipulate the heat flux [215].

It is impactful for the application of MMs on thermal management, which uses the effective combination of low thermal conductivity and high heat capacity while manipulating the heat current. Narayana et al. [216] developed a heat shield based on a MM engineering approach by the method of using isotropic materials alternately [181,182,217]. The thermal shield can protect a region from transient diffusive Heat flow with a heat source and a sink. Specifically, the MM shield is designed by a multilayer structure composed of concentric layers of polyimide films (Frälock, Cirlex) and copper sheets with varying thicknesses.

The design of camouflage devices needs unconventional material parameters to achieve thermal camouflage. The parameters have to meet the conditions of the inhomogeneity in the coordinate-transformation designs or the singularity in the bilayer-cloak designs. A thermal camouflage device that could simulate the scattering signature of a predetermined object in the environment, based on a many-body local-field effect [218]. Moreover, the many-particle metasurface of the device consists of conventional particles based on natural materials without special planning of material parameters. The thermal scattering signature of an object can be simulated by the many-particle structure and camouflage that of the default object when the object is replaced by a many-particle structure with well-designed effective thermal conductivity.

#### *The arrangement and formation of TMMs*

TMMs are artificial structures composed of several regular materials with the periodic geometry arrangement designed by transformation thermodynamics that could manipulate thermal energy and heat flux [219,220]. The materials used for forming TMMs were popular. And the reasons of TMMs possess special thermal performances were the materials possess different thermal conductivity and reasonable geometrical design and arrangement, as shown in Fig. 10. Because of the multi-material, complex geometry and arrangement, traditional manufacturing technologies were difficult in manufacturing the TMMs. AM is a popular manufacturing technology to form complex structures that are difficult to realized by traditional methods. And AM possesses unique advantages in high precision, composite structures and materials and design freedom. It is required to design an arti-

**FIGURE 10**

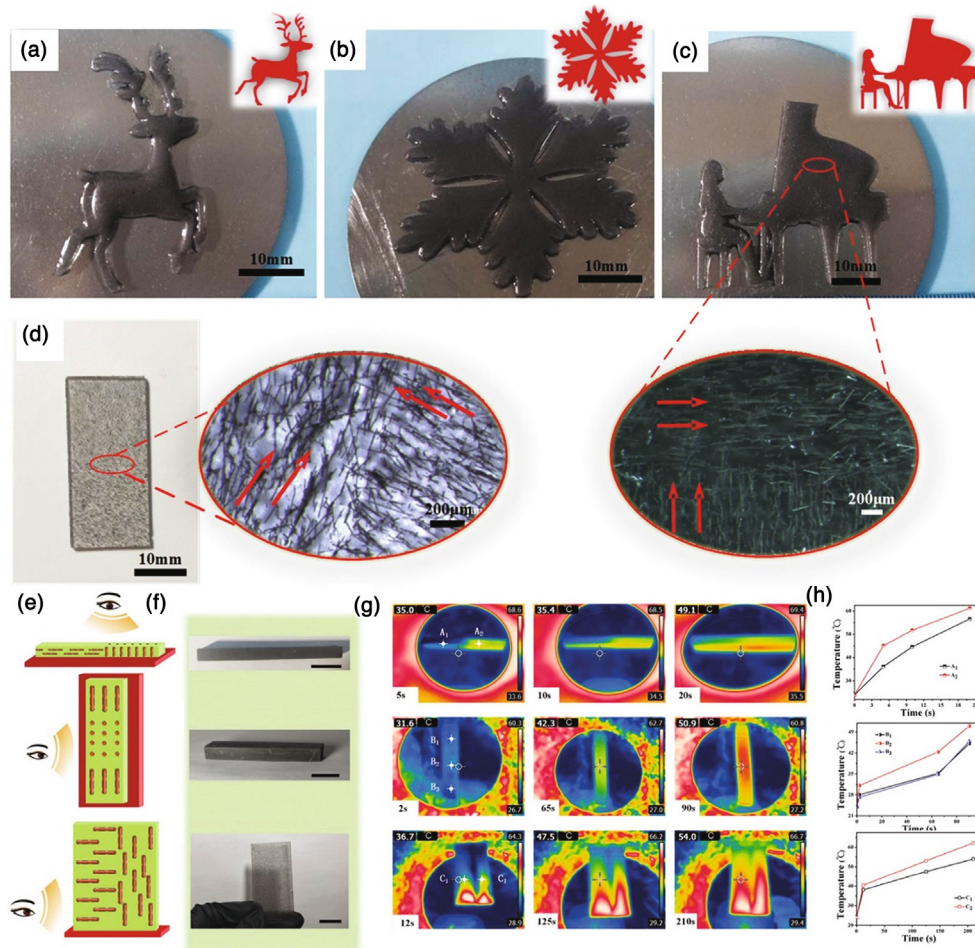
(a) Schematic diagram of a bilayer, graded structures, multi-layered and graded rings [196]. (b) Anisotropic thermal shield and cross-sectional schematic for the multilayered thermal concentrator [182]. (c) Schematic illustration of the 3D and 2D bilayer thermal cloak with naturally available materials. Experimental setup for the 2D bilayer thermal cloak [185]. (d) Fabrication of a 3D thermal cloak [187].

ficial material possessing anisotropic thermal conductivity to control the energy transport path through thermal conduction. An effective method is to design a reasonable geometrical structure and an available arrangement stacked composite from macroscopic layers of isotropic materials.

The heat conductivity of copper is higher than that of other materials, and Cu was a popular material used in TMMs such as thermal cloak and thermal inverter. It is shown in Fig. 10 that several arrangements of common TMMs. On the condition of two metal materials, a 3D thermal cloak was realized by punching a thin Cu disk into the hole of the stainless steel block via multi-material 3D printing by [187]. As for the composite of metal materials and polymers, the complex porous structures made by copper could process by SLM and filled with PDMS to realize a functional thermal cloak [181]. As shown in Fig. 10(b), the cylindrical material shield designed by 40 alternating layers of 0.36 mm thick natural latex rubber film filled by 0.38 mm thick silicone elastomers is an available TMM fabricated by a con-

ventional method. The thermal shielding was efficient as that composed of a copper cylinder. The potential process is made by UV-curing and could realize the function of control heat flow and the formation of the thermal inverter [182,190]. As shown in Fig. 11, a stereolithography 3D magnetic printing process was used to fabricated a TMM with controllable thermal conductivity. The composite materials, photocurable resins as matrix and rod-like NiCFs as reinforcing particles, were chosen. The result showed that it can adjust the thermal conductivity and thermal expansion properties by controlling the orientation of the aligned NiCFs. The proposed 3D magnetic printing strategy for manufacturing composites TMMs showed a broad application prospect in heat conduction fields [221].

In general, the TMMs are anisotropic composite structures realized by alternatively stacking two different materials that have isotropic thermal conductivity or other thermal physical properties. Using AM technology to prepare MMs can increase manufacturing flexibility, give full play to its advantages in

**FIGURE 11**

(a–d) Optical image and OM image of printed samples with site-specific fiber orientation. The red arrows represent the direction of the fiber alignment under a magnetic field. (e) Schematic illustration of composites with different fiber orientation configurations. (f) Optical images of NiCF/photosensitive resin composites. Scale bars are 20 mm. (g) Infrared thermal images of composites with different fiber alignment configurations during the heating process. (h) The surface temperature variations of composites over time [221].

structure manufacturing, and achieve integrated structure and function manufacturing. TMMs depend on the reasonable multi-layer materials distribution and structure design, and AM technology is suitable for the complex structure. As for stacking different materials, multi-material AM technology has great application prospects. As a result, AM technology can fabricate many complex TMM structures designed, realize the integrated manufacturing of TMM structure functions. It provides a new method for the design and manufacture of TMM structure devices based on functional requirements.

#### Mechanical metamaterials

MMMs is a branch of MMs which achieve the properties that can't realize in conventional materials, MMMs aim to get fantastic (zero or negative) mechanical parameters, including Poisson's ratio, modulus, etc. Simultaneously, MMMs can also achieve the mechanical goal of "super light and super strength" [222]. Conventional methods of fabricating porous MMs include melt gas injection [223], investment casting [224], physical vapor deposition [225], and sheet metal technology [226]. However, due to most MMMs need precisely control the volume fraction and

the fine internal architecture so that these MMMs are hard to achieve through the above methods. Thanks to the AM technologies with the figuration of high-accuracy and forming small parts, which give MMMs more possibility for realization and optimization. It's found that the foam structure with lateral expansion showed an NPR when stretched [227], which has a significant influence on the mechanical properties [228,229]. The above study proved that researching porous MMMs was of great significance.

#### Lightweight and energy absorption

Nearly all metals have a mass density above 1000 kg/mm<sup>3</sup>. To reduce the mass while maintaining the strength, a porous structure was introduced to solid bulk and form lattice structure to achieve lightweight. The lattice structure consists of periodic arrangement units. The light-weight structure can also absorb mechanical energy, exchange heat and possess moderate strength. For this reason, it has been used as energy absorption and biomedical scaffolds [134,230–232]. At first, Gibson and Ashby et al. [233] revealed that the mechanical performance of lattice structures was related to their volume fraction. Actually,

the effect of volume just takes apart for MMMs and researchers want to get higher mechanical properties with light-weight. It is easy to understand that Young's modulus and yield strength of lattice structures are proportional to the volume fraction. Based on the above figure, researching kinds of lattice structures to achieve light-weight as well as high strength, energy absorption become an interesting topic.

To decrease volume fraction, avoid material waste, and simultaneously get excellent mechanical performance, the simple cubic (SC), body-centered cubic (BCC) and face-centered cubic (FCC) lattice structures are introduced into the internal hollow beam [234]. The models were shown in Fig. 12(a) and could control mechanical properties, including anisotropy, Poisson's ratio, etc., by changing the ratio of the internal radius and outer radius. Simultaneously, the mechanical response of lightweight truss metal oxide lattice was researched using stretch and compression-dominated design method, which highly improved the stability and load-bearing capability (Fig. 12(b)) [235]. Furthermore, it revealed that introducing hollow lattice as reinforced honeycomb could be used for crushing protection compared to structures composed of ribs and hollow lattice trusses due to the higher energy absorption (Fig. 12 (c)) [236]. The above results all show that the lattice structure directly affects the lightweight and horizontal energy

absorption capacity, and the hollow structure has a higher level of lightweight.

The hollow structure does decrease the volume fraction, but the specific structure will introduce more sharp corners, which will cause stress concentration. The TPMS structure (Fig. 12(d and e)) could solve the problem for its curvature of any point on the surface is 0, which had a promising application in biological implants [240–242]. It is proved that TPMS is identical with trabecular bone and contribute to the differentiation of stem cell when applied in the human body [243]. Excellent mechanical properties and application prospects attracted more researches to focus on TPMS structure. For example, graphene with TPMS structure was utilized to manufacture light-weight material and verified the great mechanical performance [244–246].

The Gyroid-type TPMS lattice structures were fabricated via SLM and fatigue behavior was tested [247]. The results showed that, due to the smooth surface, the stress was uniformly distributed in different parts of the sample, leading to great fatigue resistance performance. Three kinds of TPMS-based porous structures with functional grades along the z-axis were studied by simulation [237]. The results showed that TPMS-based lattice structure transmitted stress better than conventional solid porous lattice structure, and it not only achieved light-weight but also had similar properties with natural bone

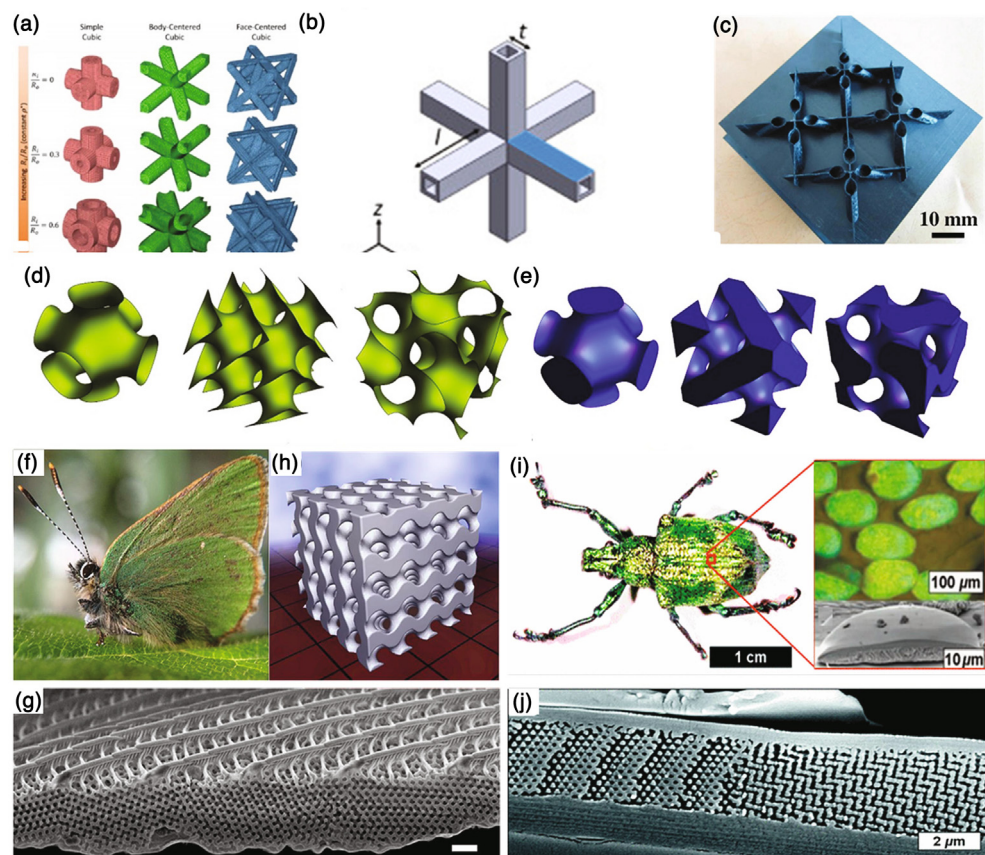


**FIGURE 12**

(a) The geometry of the elementary cubic lattices at a relative density of  $\rho^* = 0.3$  for increasing the inner to outer radius ratio [234]. (b) The geometry of hollow-truss lattice, blue area bears bending [235]. (c) The honeycomb lattice introduces a hollow structure. (d) The triangulation of non-closed implicit surface. (e) Triangulation of typical closed implicit surface [237]. (f) The butterfly in nature. (g) The microstructure of the butterfly wing. (h) TPMS-based lattice structure adapted from the butterfly wing [238]. (i) The weevil *L. augustus* in nature. (j) Detailed cross-sectional SEM image of a region of a scale [239]

tissue. The investigation on the failure mechanism of TPMS cellular structures fabricated by Vat photopolymerization AM technology under compressive loadings and verified Schwarz P structure possessed higher cyclic compressive endurance and number of cycles to failure than Gyroid structure [248]. Such a technique can provide parts with a high-resolution and smooth surface, and do not have the “layer by layer of texture” that often appears in other AM technologies and won’t cause additional local stress due to print quality compared to FDM. TPMS-based lattice structures were also found in the butterfly wings shown in Fig. 12 (f-h) and weevil *L. augustus* shown in Fig. 12 (i and j) [238,239].

Based on the characteristics of lightweight and high-energy-absorbing MMs, it is mainly used in large-scale and high-strength parts such as aircraft landing gears and wings. Therefore, the designed structure is mainly made of metallic materials, and SLM technology can prepare lightweight high-strength alloy components such as Ti6Al4V, AlSi10Mg, and shape memory alloys such as NiTi, etc. Generally speaking, it is possible to turn tens of thousands of parts into dozens of parts, reducing the weight of the airplane by 60% when using AM technologies to make airplanes and cars and thus the effective load of the airplane is greatly increased. Not only that, FDM and SLA can fabricate parts using composite materials such as non-metallic polymers. Based on the characteristics of the material itself, it can further increase the level of lightweight. At the same time, based on the polymer’s higher elastic properties and the feature of being difficult to break, it can be used to manufacture components with energy absorption, such as the sole of sports shoes that can provide a comfortable and soft feeling.

#### Zero or negative Poisson’s ratio

Why the zero or negative Poisson’s ratio materials possess great development prospects? When the material is subjected to indentation resistance, it will shrink locally, so it can well resist the local indentation resistance; when the material is bent, the material exhibits an “arch” shape, which can well resist the bending deformation. Works of literature have shown that this kind of material possesses many advantages compared to conventional counterparts. Moreover, some physical properties with strong potential engineering applications are greatly improved, including hardness [249], shear resistance [250] and energy absorption [251]. Hence, The NPR material was employed by NASA/Boeing for aviation and aerospace applications [252], which represents the figuration of a negative ratio is worth research. Lots of structure with zero or negative ratio Poisson’s ratio was created in the last decades.

Hexagonal honeycomb structure was widely used in sandwich panels for its light mass, and high specific strength, which also produced an anticlastic or saddle-shaped curvature while it bent out of plane due to the positive Poisson’s ratio. To enhance its ability of deformation, an NPR structure could be achieved by concaving two corners of a hexagonal honeycomb structure’s diagonal to the inside [7], as shown in Fig. 13(e and f). Furthermore, by changing the variable of the cell shape, the domed or synclastic curvatures could be adjusted naturally [253]. The honeycomb simultaneously possessed both hexagonal symmetry and 2D chiral symmetry, named chiral honeycomb, which was

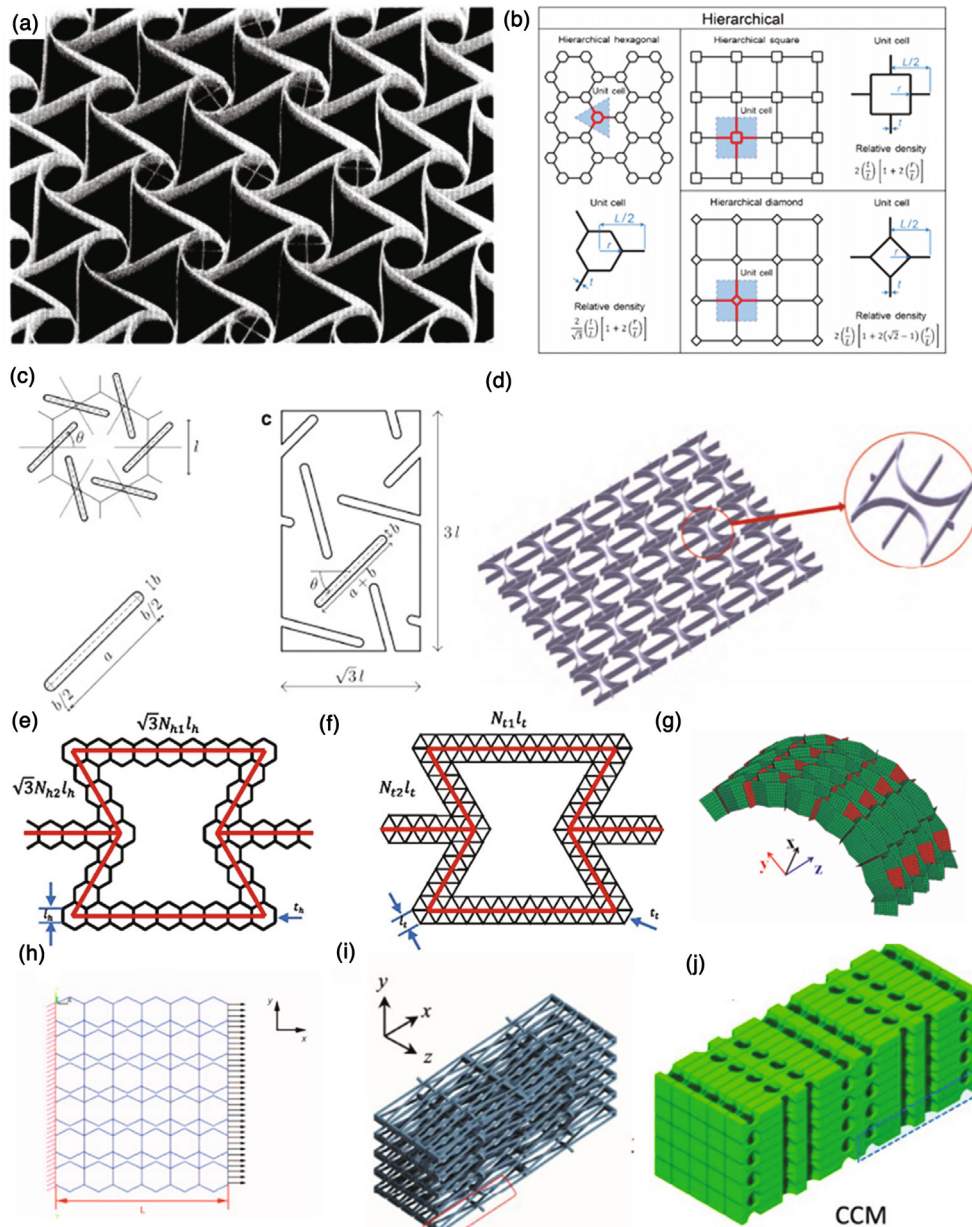
shown in Fig. 13 (a). Composed of circular elements and straight ligaments or ribs, a circular node was evenly tangent in arcs by six straight ligaments or ribs. Mousanezhad et al. [8] revealed the mechanical performance of several types of chiral honeycomb lattice structures. Moreover, he added a new variable factor compared to conventional chiral honeycomb, i.e., square elements (Fig. 13 (b)). However, the above chiral honeycombs all have ribs and elements bonding. The stress concentration of the entire structure will quickly become prominent when any one of the ribs or elements is damaged, resulting in reducing the life and carrying capacity of the structure.

Giorgio et al. [10] proposed an isotropic porous structure with an NPR in every direction (Fig. 13(c)). The auxetic cellular configuration increased in-plane shear modulus and enhance indentation resistance compared with conventional cellular structures [227,253,259,260] and the unconnected porous beam can decrease the stress concentration of the structure once a beam is damaged.

A new type of 2D ring honeycomb core structure [9], adapted from honeycomb conventional re-trant honeycomb structure and shown in Fig. 13(d). The re-entrant honeycomb structure is more stable and decreases the stress concentration with the introduction of a semi-annular wall panel compared to a conventional concave hexagon honeycomb core. The author changed the structural parameters to achieve controlled Poisson’s ratio with positive or negative. Tan [255] also re-designed conventional re-entrant honeycomb structure by introducing polygon on the ribs which improve the energy absorption and lightweight, the combination of re-entrant honeycomb structure and polygon was shown in Fig. 13(e and f).

Curved Kirigami SILICOMB cellular structures with zero Poisson’s ratio for large deformation was proposed and shown in Fig. 13(g), which possess curved radian [256]. The cellular structures with zero Poisson’s ratio can avoid anticlastic and synclastic curvature behaviors, which contribute to manufacturing the core of tubular structures [257] including air intakes, meanwhile, the curved radion causes the 2D structure to transform into a 3D which expanded practical applications. The waterjet cutting instead of AM technology was utilized to manufacture the above structure for the consideration of low-resolution requirement, time-saving and expense. Furthermore, the topology optimized architectures with programmable Poisson’s Ratio over large deformations were studied in-depth [261]. The authors achieve controllable positive or NPR and smooth transition of sharp corners. Simultaneously, the topology optimization further improves the capacity of energy absorption.

With the development of the hexagonal honeycomb structure, gradually stiffer MMs have both NPR and gradually increasing stiffness, possessing a great application prospect in cushioning and vibration damping in engineering. However, the single improvement of the hexagonal honeycomb structure can’t fulfill the mechanical properties which seriously affect the actual application. Thus, the combination of regular hexagonal honeycomb cells and auxetic honeycomb cells with NPR was studied and generated a hybrid honeycomb cell, named accordion honeycomb core [257]. Fig. 13(h) is the periodic arrangement and the deformation performance while applied axis force.

**FIGURE 13**

(a) Photograph of deformed honeycomb [254]. (b) The structure and the unit cell, and the expression of relative density for hierarchical honeycombs [8]. (c) The geometry of the porous auxetic unit cell [10]. (d) The periodic structure of circular honeycomb core [9]. (e and f) Re-entrant hierarchical honeycombs with hexagon substructure and re-entrant hierarchical honeycombs with triangle substructure [255]. (g) The model of the curved SILICOMB configuration [256]. (h) The periodic arrangement of the combination of conventional hexagonal honeycomb cell with re-entrant hexagonal honeycomb cell [257]. (i) Synthesis of a compliant porous structure. (j) A compliant cellular material with tessellated CPSes [258].

KwangwonKim et al. [258] synthesized an MMMs with variable stiffness and multiple Poisson's ratios in different directions. The author combined a regular hexagonal honeycomb on one plane with a re-entrant hexagonal honeycomb on the orthogonal plane for achieving a construct orthotropic lattice structure that possesses a controlled Poisson's ratio, including positive and negative value. The authors fabricated the structure by poly-jet based 3D printing, which provided a dimensional accuracy of 0.1% and obtained the experimental results approximately the same as the simulation results. The above structure is a combination of honeycombs along with the longitudinal and vertical directions respectively (Fig. 13(i and j)). Zhang et al. [282] pro-

posed an isotropic interpenetrating composite with either positive, zero, and negative Poisson's ratio which introducing a self-connected fiber-network and without porous result in strengthener property compared to conventional particle composites. The methods have transformed the lattice structure from 2D to 3D and further improve strength and energy absorption.

It can be seen that the research on NPR has changed from a 2D structure to a 3D structure. When the NPR material is used to make sandwich panels, it expands outwards when stretched. The material with a positive Poisson's ratio is dented inwardly and destroyed. Therefore, the safety of the lattice structure made of NPR-MMMs is greatly improved which has a wide application in

protection from striking. Besides, when NPR-MMs are fabricated by smart materials that can react to external stimulation, such as shape memory alloy, liquid crystal elastomer, and so on, some more fantastic properties will generate. For example, the idea that the NPR-MMs made by shape memory alloy can be used in solar panel frame for spacecraft. It will shrink to a small volume when in the shade, and unfold when exposed to the sunlight due to the stimulation of heat from the sun, thus more solar energy will be captured. Mark A. et al. [44] used smart materials to fabricate a Miura origami pattern with NPR via multi-material multi-nozzle 3D printing and achieved great performance.

However, the manufacturing materials are still limited to materials that are not easy to break, such as polymers. At the same time, the manufacturing accuracy of FDM has a layer of microscopic bumps or depressions compared to SLA, which is likely to cause stress concentration, while the dimensional accuracy of SLA can be 0.1%. Therefore, it can be used to produce negative Poisson's ratio structures.

#### *Vanishing shear modulus*

The Poisson's ratio is concerned with the stiffness of material for uniform isotropy material., it is easy to change the volume but difficult to change shape for NPR MMs. Young's modulus and Poisson's ratio were examined on conventional and re-entrant copper foams by resonant ultrasound spectroscopy [262], which illustrated that it is hopeful to achieve a low shear modulus. Jin et al. [64] measured the shear resistance of auxetic chiral MMMs, which applied a picture frame apparatus around the chiral structure and compressed along the direction of inclined 45°. This kind of 3D MMMs can be regarded as ideal fluid, the shear modulus  $G$  is approximately zero compared to the bulk modulus  $K$ . In other words, the characteristic of such a structure is hard to be compressed but easily flow. In the present study, the developed structures could be divided into 2 categories, that is, the pentamode structure and a kagome lattice.

All conceived MMMs can be synthesized based on pentamode materials, which can easily prevent the combination of compressional and shear waves. The parameter  $G$ ,  $K$  and Poisson's ratio  $\nu$  meet the following relationship [263]:

$$\nu = \frac{3 - 2(G/K)}{2(G/K) + 6} \quad (5)$$

Under the condition of  $G \ll K$ , the value of Poisson's ratio is 0.5. Zhang et al. [65,264] fabricated 2D PMMs via SLM and experimentally demonstrated the aforementioned theory. The artificial crystal with diamond symmetry and shown in Fig. 14 (a and b) and was fabricated with the size of  $261 \times 261 \times 224 \mu\text{m}$  by DLW, which had a filling fraction of 1.5%. It was found that diamond-type 3D pentamode materials can decouple the mass transport and mechanical properties [265], which meant that the permeability, important for the bone cell growth, of the bone scaffold made by pentamode materials could be adjusted without changing the mechanical properties.

Another PMMs structure with a cross-section shape of a regular triangle was proposed, including square, pentagon, hexagon and circle shown in Fig. 14 (c) [268]. For a typical type of PMMs (diamond type), the lattice constant was defined as an FCC struc-

ture. Furthermore, the various cross-section can also achieve nearly vanish shear modulus  $G$ . The main idea of PMMs was that there was only the normal stress without shear elements in the stress tensor when the ratio of the integral stress and prescribed stress was set as constant. According to this theory, we can use the bulk of materials with completely arbitrary elastic characteristics to prepare PMMs [269].

The kagome lattice is another structure with vanishing shear modulus with rotational triangles of a geometry shape [270–272], and it was verified the kagome structure with superior stiffness and stable lattice [273]. In the last decades, lots of researchers further studied kagome lattice[224,274,275] and demonstrated the existence of topological soft modes while positioned at desired locations in a MM, which could robustly obtain a wide range of structural deformations or variation in material parameters [276]. The C3v twist kagome lattice [275] is adapted from the conventional kagome lattice and looks simple shown in Fig. 14(d–g). The kagome lattice is isotropy with a small bulk modulus and can be regarded as zero. The distortion structure has the features of vanishing bulk modulus and NPR [277,278], this structure highly depends on boundary conditions and the performance of kagome distortions [277].

The periodical lattice structures adapted from kagome lattices with rigid triangular plates are shown in Fig. 14(h–k) [267], which produce a deformed kagome lattice by introducing a point on the square lattices with a primitive vector, including four-coordinated points and exhibited specific regions of triangle or pentagon. A periodical arrangement can help locate the desired position in the MM because the existence of dislocation will lead to insensitivity to the deformation or changes in material parameters [276,279,280]. From the viewpoint of microstructure, dislocation can help robust information storage due to the existence of presence or absence of soft mode in topological structure. Polarize isotropic exist in dislocation with the Burgers vector control the orientation.

The aim of vanishing shear modulus is to design the effective shear modulus approximately zero while comparing to bulk modulus which makes the material similar to the liquid with near-flowing figuration. PMMs can be used in an acoustic application, light-weight material et al. However, the special material was limited in 2D structure, which influences the application on the 3D layer, consequently, the 3D PMMs need to be further explored. Currently, 3D kagome lattices structure can be exchange to stacked cellular MM or twist triangular, for this reason, various industrial are encourage the study of the MMM. The research of MM of vanishing modulus will not be restricted by AM technologies, we can manufacture components from micrometers to meters, Not only that, the continuous development of simulation technology can predict the changes in the molten pool and the changes in powder during SLM forming. The powerful combination of computer simulation and AM forming MMs has also become a new method.

#### **Limitations and development tendency**

In the recent 20 years, the researches of the MMs, especially in the fields of electromagnetics, acoustics, thermotics and mechanics, have achieved great progress. Varieties of creative

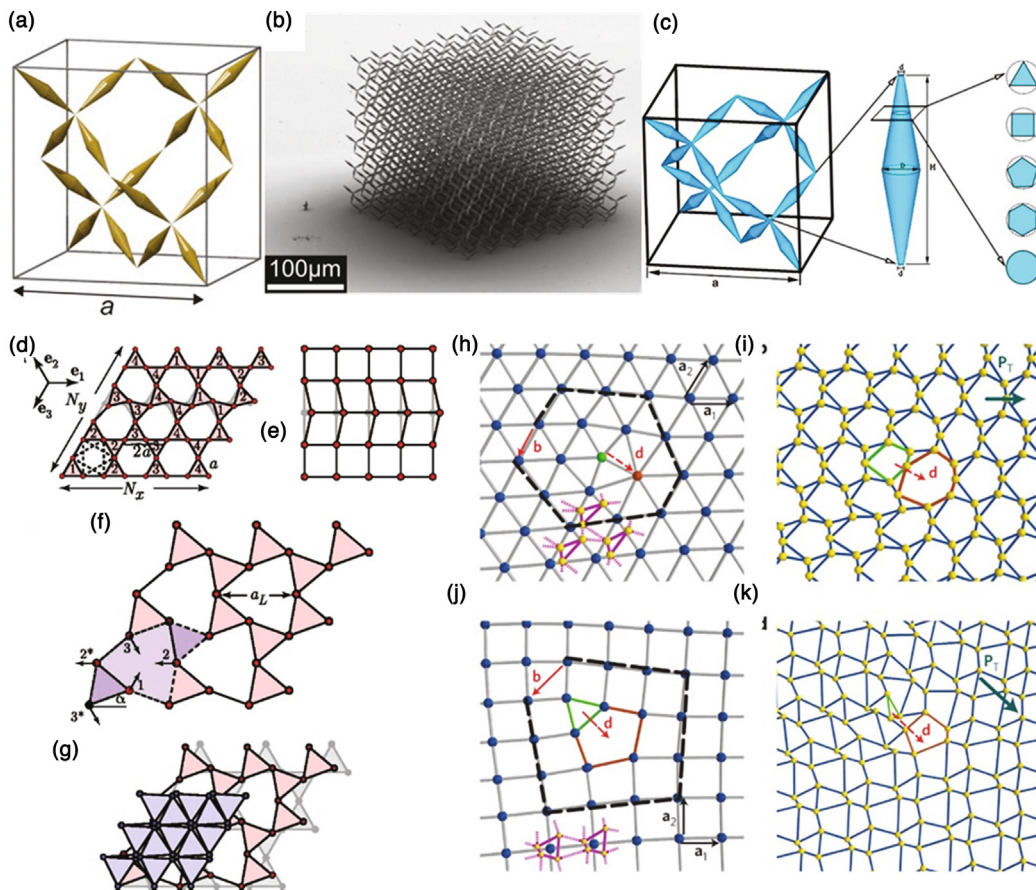


FIGURE 14

(a) The PMM proposed by Milton. (b) The fabricated sample of PMMs. [266] (c) Oblique-view electron micrograph of polymer PMMs [266]. (d–g) Cross-section of a kagome lattice three-site unit cells exist partial rotation [275]: (d) Section of a kagome lattice with  $N_x = N_y = 4$  and  $N_c = N_x N_y$  three site unit cells. (e) Section of a square lattice depicting a floppy mode in which all sites along a line are displaced uniformly. (f) Twisted kagome lattice. (g) Superposed snapshots of the twisted lat showing decreasing areas with increasing  $\alpha$ . (h) the hexagonal lattice with primitive vectors ( $a_1, a_2$ ). (i) Deformed hexagonal lattice adapted from (h). (j) The topological polarization. (k) corrected each point in (h) with the four-point unit cell (yellow points and magenta bonds) [267].

microstructures were come up with to achieve exotic properties that cannot be found in nature, such as negative refractive index, invisibility from the detectors with the electromagnetic or acoustic waves acting as the information medium, et al. These fantastic products have a broad application prospect in both national defense industry and people's livelihood field. In recent decades, kinds of AM technologies, such as SLS, SLM, SLA, FDM, TPM, etc. were developed to meet the fabrication of the complicated structure of different materials including ceramics, metals and polymers. Furthermore, the forming efficiency and precision of AM technologies are also getting higher and higher, which provides a more ideal method to fabricate the MMs samples and promote their application in various situations.

Despite such great achievements, a lot of work remains to be done to achieve higher performance. In the aspect of MMs design, an overarching challenge is to broaden the dimensionality of MMs from 2D to 3D. The existed MMs are mainly designed in 2D and achieve great simulation and experiment effect. But in the practical application, the 2D MMs will suffer total failure in the direction perpendicular to the 2D plane. However, the transformation of the structure design from 2D to 3D is not an easy job, the design method of 2D structures

may not be applicable at all when the dimension rises to 3D. For example, the gradient cylindrical structures can realize 2D ACMs with gradual physical parameters while failing in a 3D situation, thus a new structure design method is needed to satisfy the new demand.

On the other hand, though there are a few reports of 3D MMs, most of them are anisotropic. For example, the structure of the current 3D ACMs is designed as a pyramid [140,281], which could achieve a cloaking effect as the incident wave is parallel to the axis. When the incident sound wave deviates from the set direction, the designed ACMs will be visible to the acoustic detector. Moreover, many current MMs only work at a specific condition, which cannot satisfy the variable external environment. For example, the EMMs and AMMs are effective in a limited frequency range, sometimes only a dozen hertz, which limits their practical application. Therefore, it's a challenging task to break through the inherent limits of MMs.

In addition to overcoming the shortcomings mentioned above, there are also some promising directions for the future research of MMs. Though MMs are roughly divided into 4 categories in this paper, their functions are not limited. The functions of different types of MMs can be combined. The versatile MMs can be realized by making use of the structural

characteristics and the properties of materials themselves. For example, the decorated membrane resonator AAMs proposed by Ma [154] can not only achieve a certain frequency range of sound absorption, but also convert part of the sound energy into electrical energy, and realize a conversion rate of up to 23%. Another promising work is to fabricate MMs with smart materials (that can react to external stimulation, such as shape memory alloy, liquid crystal elastomer, etc.) via AM technologies. The physical parameters of MMs will change with the variation of external stimulation, thus the function can be adjusted through carefully designing the structure and controlling the stimulating condition.

In the aspect of MMs fabrication, AM technique is a relatively ideal option for MMs with complicated structures, which can reduce the manufacturing process, simplify and automate the design – manufacturing procedure, and save lots of labors. However, the applications of AM technologies in MMs also face some limits:

- (i) The current AM technologies perform not very well in manufacturing multi-material, which is limited by its forming principle. Moreover, in order to satisfy the gradient physical parameters of MMs, the properties of different materials are usually quite different, making it difficult to achieve effective interface bonding. This is why the relatively mature multi-material AM technologies, such as SLA and FDM, also face difficulties in manufacturing multi-material MMs.
- (ii) Supports of complex structures are difficult to remove. As AM technologies rely on a layer by layer manufacturing, the supporting structure is needed to ensure the forming accuracy while forming a complex structure. When the structure is too complex or the structure size is too small, the supporting structure is difficult to remove, thus the performance of MMs will be discounted.
- (iii) The acute contradiction between size and resolution. Some micro-AM technologies, such as TPM, enable accurate fabrication of nano-scale structures, but fail to manufacture large size ones. This, in turn, imposes some constraints on the design of MMs. In addition, AM technologies with different resolution have specific materials for which they are applicable, and when both materials and resolution constraints are considered, AM technologies may not be ideal solutions.

In recent years, great progresses have been made in AM technologies, especially in multi-material and micro-printing, gradually solving some of the limitations mentioned above. Traditional AM technologies are based on a layer-by-layer approach, where each layer can be regarded as a basic unit. That concept was turned on its head in the work published in *Nature* in 2019 [44]. The basic unit of AM is no longer a sheet, but a voxel, which allows structures or materials to have richer properties, and even a soft robot could be print directly. In terms of micro-printing, the TPP has been able to achieve nano-scale printing but low efficiency. Newly developed volumetric 3D-printing [281] on the basis of micro-scale manufacturing precision, forming efficiency is higher than the TPP four to five orders

of magnitude. The future of AM technologies will be in the direction of ultra-large, ultra-fine, multi-material and faster fabrication.

## Summary

In summary, we have briefly introduced the principles and the development process of four types of MMs, EMMs, AMMs, TMMs and MMMs, and the application status of AM technology in typical MMs. The extraordinary properties of MMs, such as negative/zero Poisson's ratio, negative refractive index, etc., can be realized by carefully designing the microstructures that determine the physical parameters of the MMs. Though the present MMs still have lots of limits and shortcomings, these exotic properties make them prospect in many fields like national defense, aviation, buildings and others, which attract many researchers to devote in. Moreover, the continuous progress of AM technology will promote the development and application of MMs.

## Declaration of Competing Interest

The authors declare that they have no known competing financial interests or personal relationships that could have appeared to influence the work reported in this paper.

## Acknowledgments

This work was sponsored by the Natural and Science Foundation of China (Grant No. 51922044, 51775208), the Academic frontier youth team (2017QYTD06, 2018QYTD04) at Huazhong University of Science and Technology (HUST). The authors thank the Analytical and Testing Center of HUST for SEM examination and the State Key Laboratory of Materials Processing and Die & Mould Technology for compression tests.

## References

- [1] S. Obrien et al., *J. Phys.: Condens. Matter* 14 (25) (2002) 6383–6394.
- [2] J.B. Pendry et al., *Science* 312 (5781) (2006) 1780–1782.
- [3] D. Schurig et al., *Science* 314 (5801) (2006) 977–980.
- [4] L.W. Cai et al., *New J. Phys.* 9 (12) (2007) 450.
- [5] S.A. Cummer et al., *New J. Phys.* 9 (3) (2007) 45.
- [6] R. Lakes, *Science* 235 (4792) (1987) 1038–1040.
- [7] I. Masters et al., *Compos. Struct.* 35 (1996) 403–422.
- [8] D. Mousanezhad et al., *Theor. Appl. Mech. Lett.* 6 (2) (2016) 81–96.
- [9] W. Jiang et al., *Chin. Sci. Bull.* 61 (13) (2016) 1421–1427.
- [10] G. Carta et al., *Mech. Mater.* 97 (2016) 67–75.
- [11] V.G. Veselago, *Physics-Uspokhi* 10 (4) (1968) 509–514.
- [12] R.A. Shelby et al., *Science* 292 (5514) (2001) 77–79.
- [13] J. Li et al., *Phys. Rev. E Stat. Nonlin. Soft Matter Phys.* 70 (5 Pt 2) (2004) 055602.
- [14] D.R. Smith et al., *Science* 305 (5685) (2004) 788–792.
- [15] Z. Chen et al., *Physica B: Condensed Matter* 438 (2014) 1–8.
- [16] E. Yablonovitch, *Phys. Rev. Lett.* 58 (20) (1987) 2059–2062.
- [17] S. John, *Phys. Rev. Lett.* 58 (23) (1987) 2486–2489.
- [18] J.B. Pendry et al., *IEEE T. Microw. Theory* 47 (11) (1999) 2075–2084.
- [19] R.M. Walser et al., Electromagnetic metamaterials. Presented at Complex Mediums II: Beyond Linear Isotropic Dielectrics, (2001)
- [20] Q. Cheng et al., *New J. Phys.* 12 (6) (2010) 063006.
- [21] H.W. Wang et al., *J. Appl. Phys.* 109 (10) (2011) 103104.
- [22] C. Luo et al., *J. Alloys Compd.* 652 (2015) 18–24.
- [23] N.I. Zheludev et al., *Nat. Mater.* 11 (11) (2012) 917–924.
- [24] T. Nagatsuma et al., *Nat. Photonics* 10 (6) (2016) 371–379.
- [25] E. Philip et al., *J. Infrared Millimeter Terahertz Waves* 38 (9) (2017) 1047–1066.
- [26] Z. Liu et al., *Science* 289 (5485) (2000) 1734–1736.
- [27] L. Fok et al., *MRS Bull.* 33 (10) (2008) 931–934.
- [28] A.N. Norris, *Proc. R. Soc. London, A* 464 (2097) (2008) 2411–2434.
- [29] S. Zhang et al., *Phys. Rev. Lett.* 106 (2) (2011) 024301.

- [30] W. Kan et al., *Phys. Rev. Appl.* 3 (2015) 6.
- [31] L. Zigmoneanu et al., *Nat. Mater.* 13 (4) (2014) 352–355.
- [32] Z. Liang et al., *Phys. Rev. Lett.* 108 (11) (2012) 114301.
- [33] M. Fink, *Nat. Mater.* 13 (9) (2014) 848–849.
- [34] M. Yang et al., *Mater. Horiz.* 4 (4) (2017) 673–680.
- [35] C.R. Liu et al., *Appl. Phys. Express* 12 (2019) 8.
- [36] D. Torrent et al., *New J. Phys.* 9 (9) (2007) 323.
- [37] J. Chen et al., *Nat. Commun.* 9 (1) (2018) 4920.
- [38] D.C. Chen et al., *Appl. Phys. Lett.* 115 (8) (2019) 083501.
- [39] R. Lakes, *Science* 238 (4826) (1987) 551.
- [40] K.E. Evans et al., *Nature* 353 (1991) 124.
- [41] W. Wu et al., *Mater. Design* 180 (2019) 107950.
- [42] G. Wei et al., *Phys. Rev. E* 58 (5) (1998) 6173–6181.
- [43] M. Askari et al., *Additive Manuf.* 36 (2020) 101562.
- [44] M.A. Skylar-Scott et al., *Nature* 575 (7782) (2019) 330–335, <https://doi.org/10.1038/s41586-019-1736-8>.
- [45] M. Regehly et al., *Nature* 588 (7839) (2020) 620–624.
- [46] L. Hirt et al., *Adv. Mater.* 29 (2017) 17.
- [47] D. Oran et al., *Science* 362 (6420) (2018) 1281–+.
- [48] B.E. Kelly et al., *Science* 363 (6431) (2019) 1075–1079, <https://doi.org/10.1126/science.aau711>.
- [49] S.K. Saha et al., *Science* 366 (6461) (2019) 105–+.
- [50] J.R. Tumbleston et al., *Science* 347 (6228) (2015) 1349–1352.
- [51] M. Vaezi et al., *Int. J. Adv. Manuf. Technol.* 67 (5–8) (2012) 1721–1754.
- [52] G. Yoon et al., *Sci. Rep.-UK* 7 (2017).
- [53] A. Vyatskikh et al., *Nat. Commun.* 9 (1) (2018) 593.
- [54] Y. Liu et al., *Nat. Commun.* 10 (2019).
- [55] T. Ergin et al., *Science* 328 (5976) (2010) 337–339.
- [56] M. Yin et al., *Appl. Phys. Lett.* 100 (2012) 12.
- [57] B. Zhang et al., *IEEE Trans. Comp. Pack. Manuf. Technol.* 6 (5) (2016) 796–804.
- [58] X. Chen et al., *Opt. Laser Technol.* 124 (2020) 105972.
- [59] W.-Q. Ji et al., *J. Phys. D: Appl. Phys.* 52 (32) (2019) 325302.
- [60] M. He et al., *Small* 11 (44) (2015) 5889–5894.
- [61] J. Liu et al., *Compos. Part A-Appl. Sci. Manuf.* 120 (2019) 140–146.
- [62] Y.-G. Peng et al., *Adv. Funct. Mater.* 30 (2020) 28.
- [63] T. Buckmann et al., *Nat. Commun.* 5 (2014) 4130.
- [64] S. Jin et al., *Int. J. Solids Struct.* 174 (2019) 28–37.
- [65] L. Zhang et al., *Engineering* 6 (1) (2020) 56–67.
- [66] S. Liu et al., *Light-Sci. Appl.* 5 (2016) 5.
- [67] G.D. Bai et al., *Appl. Phys. Lett.* 107 (2015) 15.
- [68] R. Nair et al., *Science* 320 (5881) (2008) 1308.
- [69] Q. Liao et al., *J. Appl. Phys.* 122 (19) (2017) 193101.
- [70] A. Ahmadi et al., *Phys. Rev. B* 77 (4) (2008) 045104.
- [71] J.A. Schuller et al., *Phys. Rev. Lett.* 99 (10) (2007) 107401.
- [72] U. Levy et al., *Phys. Rev. Lett.* 98 (24) (2007) 243901.
- [73] M.S. Wheeler et al., *Phys. Rev. B* 72 (19) (2005) 193103.
- [74] A.N. Lagarkov et al., *Phys. Rev. B* 53 (10) (1996) 6318–6336.
- [75] H. Chen et al., *Phys. Rev. B* 78 (5) (2008) 054204.
- [76] D. Xiao et al., *Opt. Lett.* 33 (8) (2008) 860–862.
- [77] A. Houck et al., *Phys. Rev. Lett.* 90 (13) (2003) 137401.
- [78] T. Yen et al., *Science* 303 (5663) (2004) 1494–1496.
- [79] K. Bolotin et al., *Solid State Commun.* 146 (9) (2008) 351–355.
- [80] A.K. Geim, *Science* 324 (5934) (2009) 1530–1534.
- [81] K.S. Novoselov et al., *Nature* 490 (7419) (2012) 192–200.
- [82] C.R. Garcia et al., *Prog. Electromagnetics Res. Lett.* 34 (2012) 75–82.
- [83] J.A. Dolan et al., *Adv. Opt. Mater.* 3 (1) (2015) 12–32.
- [84] U. Leonhardt, *Science* 312 (5781) (2006) 1777–1780.
- [85] U. Leonhardt et al., *Prog. Optics* 53 (2008) 69–152.
- [86] J.T.H. Li et al., *Phys. Rev. Lett.* 101 (20) (2008) 203901.
- [87] J. Valentine et al., *Nat. Mater.* 8 (7) (2009) 568–571.
- [88] J. Zhou et al., *Phys. Rev. Lett.* 95 (22) (2005) 223902.
- [89] N. Yu et al., *Science* 334 (6054) (2011) 333–337.
- [90] F. Aieta et al., *Nano Lett.* 12 (9) (2012) 4932–4936.
- [91] J. Zhang et al., *Appl. Phys. Lett.* 103 (15) (2013) 151115.
- [92] N.M. Estakhri et al., *IEEE Antennas Wireless Propagation Lett.* 13 (2014) 1775–1778.
- [93] L. Hsu et al., *Prog. Electromag. Res.-pier* 152 (2015) 33–40.
- [94] B. Orazbayev et al., *Adv. Opt. Mater.* 5 (1) (2017) 1600606.
- [95] A. Bandyopadhyay et al., *Mater. Sci. Eng.: R* 129 (2018) 1–16.
- [96] W. Lu et al., *J. Appl. Phys.* 108 (6) (2010) 064517.
- [97] E.E. Narimanov et al., *Appl. Phys. Lett.* 95 (4) (2009) 041106.
- [98] C. Argyropoulos et al., *Opt. Express* 17 (10) (2009) 8467–8475.
- [99] M. Yin et al., *Opt. Express* 21 (16) (2013) 19082–19090.
- [100] Z. Yang et al., *Mater. Lett.* 151 (151) (2015) 109–111.
- [101] R. Panwar et al., *IEEE Trans. Magn.* 51 (11) (2015) 1–4.
- [102] W. Jiang et al., *Sci. Rep.-UK* 8 (1) (2018) 1–7.
- [103] H. Song et al., *IEEE Trans. Terahertz Sci. Technol.* 1 (1) (2011) 256–263.
- [104] T. Kleineostmann et al., *J. Infrared Millimeter Terahertz Waves* 32 (2) (2011) 143–171.
- [105] P.U. Jepsen et al., *Laser Photonics Rev.* 5 (1) (2011) 124–166.
- [106] W. Jin et al., *Nat. Commun.* 9 (1) (2018) 5122.
- [107] A. Von Bieren et al., Monolithic metal-coated plastic components for mm-wave applications. In international conference on infrared millimeter and terahertz waves, (2014), pp 1–2.
- [108] D.W. Vogt et al., *J. Infrared Millimeter Terahertz Waves* 37 (11) (2016) 1086–1095.
- [109] C.-S. Kee et al., *J. Appl. Phys.* 87 (4) (2000) 1593–1596.
- [110] F. Cervera et al., *Phys. Rev. Lett.* 88 (2) (2002) 023902.
- [111] D. Torrent et al., *New J. Phys.* 10 (6) (2008), <https://doi.org/10.1088/1367-2630/10/6/063015>.
- [112] D. Torrent et al., *New J. Phys.* 10 (2) (2008) 023004.
- [113] M. Farhat et al., *Phys. Rev. Lett.* 101 (13) (2008) 134501.
- [114] S.-C.-S. Lin et al., *J. Appl. Phys.* 106 (5) (2009) 053529.
- [115] S.C. Lin et al., *J. Appl. Phys.* 111 (12) (2012) 123510.
- [116] Y. Li et al., *Sci. Rep.* 4 (2014) 6830.
- [117] T. Gorishnyy et al., *Phys. Rev. Lett.* 94 (11) (2005) 115501.
- [118] G. Grynnberg et al., *Phys. Rev. Lett.* 70 (15) (1993) 2249–2252, <https://doi.org/10.1103/PhysRevLett.70.2249>.
- [119] R.H. Olsson et al., *Sensor. Actuat. A-Phys.* 145–146 (2008) 87–93.
- [120] R.H. Olsson III et al., *Meas. Sci. Technol.* 20 (2009) 1.
- [121] B.J. Ash et al., *Nat. Commun.* 8 (1) (2017) 174.
- [122] K. Yu et al., *Adv. Mater.* 30 (21) (2018) e1706348.
- [123] Y. Cheng et al., *Appl. Phys. A* 94 (1) (2008) 25–30.
- [124] M. Farhat et al., *Phys. Rev. Lett.* 103 (2) (2009) 024301.
- [125] M. Farhat et al., *Phys. Rev. B* 79 (2009) 3.
- [126] H. Chen et al., *J. Phys. D: Appl. Phys.* 43 (2010) 11.
- [127] H. Chen et al., *Appl. Phys. Lett.* 91 (18) (2007) 183518, <https://doi.org/10.1063/1.2803315>.
- [128] Y. Cheng et al., *Appl. Phys. Lett.* 92 (15) (2008) 151913.
- [129] H. Shen et al., *J. Phys. D: Appl. Phys.* 45 (28) (2012) 285401.
- [130] Q. Li et al., *Appl. Phys. Lett.* 105 (10) (2014) 101906.
- [131] Q. Wei et al., *Appl. Phys. A* 109 (4) (2012) 913–919.
- [132] Y. Urzhumov et al., *New J. Phys.* 12 (7) (2010) 073014.
- [133] Y. Yang et al., *Sci. Rep.* 6 (2016) 20219.
- [134] J. Zhang et al., *Compos. Part B: Eng.* 202 (2020) 108417.
- [135] Y. Chen et al., *Sci. Rep.* 5 (2015) 15745.
- [136] Y. Chen et al., *Phys. Rev. B* 95 (2017) 18.
- [137] A. Diatta et al., *Opt. Exp.* 18 (11) (2010) 11537–11551.
- [138] W. Hu et al., *J. Appl. Phys.* 113 (2) (2013) 024911.
- [139] Y. Bi et al., *Appl. Phys. Lett.* 112 (22) (2018) 223502.
- [140] J. Zhu et al., *Phys. Scr.* 94 (11) (2019) 115003.
- [141] P.A. Kerrian et al., *J. Acoust. Soc. Am.* 146 (4) (2019) 2303.
- [142] H.-T. Zhou et al., *Smart Mater. Struct.* 29 (6) (2020) 065016.
- [143] Z. Yang et al., *Appl. Phys. Lett.* 96 (4) (2010) 041906.
- [144] X. Cai et al., *Appl. Phys. Lett.* 105 (2014) 12.
- [145] T.Y. Huang et al., *J. Acoust. Soc. Am.* 139 (6) (2016) 3240, <https://doi.org/10.1121/1.4950751>.
- [146] C. Zhang et al., *Phys. Rev. Appl.* 6 (2016) 6.
- [147] C. Chen et al., *Appl. Phys. Lett.* 110 (22) (2017) 221903.
- [148] L. Liu et al., *Appl. Phys. Lett.* 111 (2017) 8.
- [149] S. Huang et al., *Appl. Phys. Lett.* 113 (23) (2018) 233501.
- [150] Y. Wang et al., *J. Appl. Phys.* 123 (18) (2018) 185109.
- [151] X. Wu et al., *Appl. Phys. Lett.* 109 (2016) 4.
- [152] H. Long et al., *Appl. Phys. Lett.* 110 (2) (2017) 023502.
- [153] Y. Zhou et al., *Appl. Phys. Lett.* 115 (9) (2019) 093503.
- [154] G. Ma et al., *Nat. Mater.* 13 (9) (2014) 873–878.
- [155] X. Jiang et al., *Appl. Phys. Lett.* 105 (2014) 24.
- [156] S. Huang et al., *Sci. Bull.* 65 (5) (2020) 373–379.
- [157] Silence, Products 2021 <http://www.4silence.com>.
- [158] M. Bezemer-Krijnen, Sound absorption of porous structures: a design tool for road surfaces, 2018.
- [159] B. Assouar et al., *Nat. Rev. Mater.* 3 (12) (2018) 460–472.
- [160] Y. Li et al., *Appl. Phys. Lett.* 101 (23) (2012) 233508.
- [161] Y. Li et al., *Appl. Phys. Lett.* 103 (5) (2013) 053505.
- [162] P. Peng et al., *Phys. Lett. A* 378 (45) (2014) 3389–3392.

- [163] W. Wang et al., *Appl. Phys. Lett.* 105 (10) (2014) 101904.
- [164] R. Al Jahdali et al., *Appl. Phys. Lett.* 108 (3) (2016) 031902.
- [165] S. Qi et al., *Phys. Rev. Appl.* 7 (2017) 5.
- [166] F. Ma et al., *J. Math. Chem.* 7 (17) (2019) 5131–5138.
- [167] X. Su et al., *J. Acoust. Soc. Am.* 141 (6) (2017) 4408.
- [168] E. Dong et al., *Natl. Sci. Rev.* 6 (5) (2019) 921–928.
- [169] A.C. Hladky-Hennion et al., *Appl. Phys. Lett.* 102 (14) (2013) 144103.
- [170] Y. Tian et al., *Appl. Phys. Lett.* 107 (22) (2015) 221906.
- [171] Y. Liu et al., *Chin. Phys. B* 28 (2) (2019) 024301.
- [172] W. Chong et al., *J. Acoust. Soc. Am.* 136 (1) (2014) 423–429.
- [173] Y. Zhang et al., *Appl. Phys. Lett.* 105 (12) (2014) 123502.
- [174] X. Gao et al., *Appl. Phys. Lett.* 109 (1) (2016) 013505.
- [175] Z. Song et al., *Phys. Rev. E* 93 (1) (2016) 012411.
- [176] K.P. Vemuri et al., *Appl. Phys. Lett.* 105 (19) (2014) 193904.
- [177] P. Pichanusakorn et al., *J. Appl. Phys.* 107 (7) (2010) 074304.
- [178] T.E. Humphrey et al., *Physica E* 29 (1–2) (2005) 390–398.
- [179] M. Kadic et al., *Rep. Prog. Phys.* 76 (12) (2013) 126501.
- [180] P. Pichanusakorn et al., *Appl. Phys. Lett.* 94 (22) (2009) 223108.
- [181] R. Schittny et al., *Phys. Rev. Lett.* 110 (19) (2013) 195901.
- [182] S. Narayana et al., *Phys. Rev. Lett.* 108 (2012) 21.
- [183] S. Guenneau et al., *Opt. Exp.* 20 (7) (2012) 8207–8218.
- [184] K.P. Vemuri et al., *Appl. Phys. Lett.* 104 (8) (2014) 083901.
- [185] T. Han et al., *Phys. Rev. Lett.* 112 (5) (2014) 054302.
- [186] T. Han et al., *Energ. Environ. Sci.* 6 (12) (2013) 3537.
- [187] H. Xu et al., *Phys. Rev. Lett.* 112 (5) (2014) 054301.
- [188] U. Leonhardt, *Nature* 498 (7455) (2013) 440–441.
- [189] Y. Ma et al., *Phys. Rev. Lett.* 113 (2014) 20.
- [190] M. Maldovan, *Nature* 503 (7475) (2013) 209–217.
- [191] H. Xu et al., *Phys. Rev. Lett.* 112 (2014) 5.
- [192] T. Han et al., *Adv. Mater.* 26 (11) (2014) 1731–1734, <https://doi.org/10.1002/adma.201304448>.
- [193] T. Yang et al., *Adv. Mater.* 27 (47) (2015) 7752–7758.
- [194] F.M. Canbazoglu et al., *Appl. Phys. Lett.* 106 (14) (2015) 143904.
- [195] K.P. Vemuri et al., *Appl. Phys. Lett.* 103 (2013) 13.
- [196] R. Wang et al., *J. Appl. Phys.* 123 (11) (2018) 115117.
- [197] A.V. Shchegrov et al., *Phys. Rev. Lett.* 85 (7) (2000) 1548–1551.
- [198] M. Florescu et al., *Phys. Rev. B* 75 (2007) 20.
- [199] Y. Guo et al., *Appl. Phys. Lett.* 101 (13) (2012) 131106.
- [200] Z. Jacob et al., *Appl. Phys. Lett.* 100 (18) (2012) 181105.
- [201] H.N.S. Krishnamoorthy et al., *Science* 336 (6078) (2012) 205–209.
- [202] E. Rousseau et al., *Nat. Photonics* 3 (9) (2009) 514–517.
- [203] S. Shen et al., *Nano Lett.* 9 (8) (2009) 2909–2913.
- [204] S.A. Biehs et al., *Phys. Rev. Lett.* 105 (23) (2010) 234301.
- [205] B. Liu et al., *Phys. Rev. B* 87 (11) (2013) 115403.
- [206] S.A. Biehs et al., *Opt. Express* 19 (19) (2011) A1088–A1103.
- [207] A. Alu et al., *Phys. Rev. Lett.* 100 (11) (2008) 113901.
- [208] S.R. Sklan et al., *Natl. Sci. Rev.* 5 (2) (2018) 138–141.
- [209] W. Kan et al., *Sci. Rep.-UK* 3 (2013).
- [210] N. Li et al., *Rev. Modern Phys.* 84 (3) (2012) 1045–1066.
- [211] W.X. Jiang et al., *Adv. Funct. Mater.* 23 (32) (2013) 4028–4034.
- [212] Y. Lai et al., *Phys. Rev. Lett.* 102 (25) (2009) 253902.
- [213] W.X. Jiang et al., *Phys. Rev. E* 83 (2011) 2.
- [214] J.C.M. Garnett et al., *Philos. Trans. Royal Soc. London Series A* 303 (359–371) (1904) 385–420.
- [215] T. Han et al., *Prog. Electromagn. Res.* 143 (2013) 131–141.
- [216] S. Narayana et al., *Appl. Phys. Lett.* 102 (20) (2013) 201904.
- [217] T. Han et al., *Sci. Rep.* 3 (2013) 1593.
- [218] R. Wang et al., *Int. J. Thermal Sci.* 131 (2018) 14–19.
- [219] X. Wu et al., *Smart Mater. Struct.* 28 (9) (2019) 093001.
- [220] G. Park et al., *Sci. Rep.-UK* 7 (1) (2017) 41000.
- [221] L. Ren et al., *Adv. Mater. Technol.* 4 (7) (2019) 1900296, <https://doi.org/10.1002/admt.201900296>.
- [222] X. Zheng et al., *Science* 344 (6190) (2014) 1373–1377.
- [223] J. Banhart, *Prog. Mater. Sci.* 46 (6) (2001) 559–632.
- [224] J. Wang et al., *Int. J. Solids Struct.* 40 (25) (2003) 6981–6988.
- [225] D. Queheillalt et al., *J. Mater. Res.* 16 (2001) 1028–1036.
- [226] F.W. Zok et al., *Int. J. Solids Struct.* 41 (22) (2004) 6249–6271.
- [227] R. Lakes, *Science* (New York, N.Y.) 235 (1987) 1038–1040.
- [228] J.-B. Choi et al., *J. Compos. Mater.* 29 (1995) 113–128.
- [229] W.-Y. Jang et al., *Int. J. Solids Struct.* 47 (2010) 2872–2883.
- [230] A.G. Evans et al., *Prog. Mater. Sci.* 46 (3) (2001) 309–327.
- [231] S. Arabnejad et al., *Acta Biomater.* 30 (2016) 345–356.
- [232] M. Alzahrani et al., *Mater. Design* 85 (2015) 349–360.
- [233] L. Gibson et al., *Cell. Solids: Struct. Prop.* (1997).
- [234] T. Tancogne-Dejean et al., *Extreme Mech. Lett.* 22 (2018) 13–18.
- [235] P.K. Kanaujia et al., *Materialia* 8 (2019) 100439.
- [236] S. Yin et al., *Compos. Struct.* 160 (2017) 1147–1154.
- [237] L. Li et al., *J. Orthopaedic Transl.* 19 (2019) 94–105.
- [238] R.W. Corkery et al., *Interface Focus* 7 (4) (2017) 20160154.
- [239] J.W. Galusha et al., *Phys. Rev. E Stat. Nonlin. Soft Matter Phys.* 77 (5 Pt 1) (2008) 050904.
- [240] U. Pinkall et al., *Exp. Math.* 2 (1) (1993) 15–36.
- [241] M. Zhao et al., *Materials* 11 (12) (2018) 2411.
- [242] M. Zhao et al., *Int. J. Mech. Sci.* 167 (2020) 105262.
- [243] H. Jinnai et al., *Adv. Mater.* 1450 (2002).
- [244] Z. Qin et al., *Sci. Adv.* 3 (1) (2017) e1601536.
- [245] G.S. Jung et al., *Nano Lett.* 18 (8) (2018) 4845–4853.
- [246] G.S. Jung et al., *Nanoscale* 9 (36) (2017) 13477–13484.
- [247] L. Yang et al., *Acta Mater.* 181 (2019) 49–66.
- [248] M. Keshavarzan et al., *Mech. Mater.* 140 (2020) 103150.
- [249] L.L. Hu et al., *Compos. Struct.* 207 (2019) 323–330.
- [250] J. Ju et al., *Mater. Design* 32 (2) (2011) 512–524.
- [251] J. Xiang et al., *Mater. Sci. Eng.: A* 696 (2017) 283–289.
- [252] R. Lakes, *J. Mater. Sci.* 26 (1991).
- [253] K. Evans, *Compos. Struct.* 17 (1991) 95–111.
- [254] D. Prall et al., *Int. J. Mech. Sci.* 39 (3) (1997) 305–314.
- [255] H.L. Tan et al., *Compos. Struct.* 229 (2019) 111415.
- [256] F. Scarpa et al., *J. Intel. Mater. Syst. Struct.* 25 (2013).
- [257] K. Olympio et al., *J. Intel. Mater. Syst. Struct.* 21 (2010) 1737–1753.
- [258] K. Kim et al., *Mech. Mater.* 125 (2018) 14–25.
- [259] K.E. Evans et al., *Eng. Sci. Educ. J.* 9 (4) (2000) 148–154.
- [260] G.W. Milton, *J. Mech. Phys. Solids* 40 (5) (1992) 1105–1137.
- [261] A. Clausen et al., *Adv. Mater.* 27 (37) (2015) 5523–5527.
- [262] D. Li et al., *Phys. Status Solidi B* 250 (2013) 1983–1987.
- [263] Z. Wang et al., *Appl. Thermal Eng.* 111 (2017) 122–133.
- [264] L. Zhang et al., *Compos. Struct.* 226 (2019) 111199.
- [265] L. Zhang et al., *Acta Biomater.* 112 (2020) 298–315.
- [266] M. Kadic et al., *Appl. Phys. Lett.* 100 (19) (2012) 191901.
- [267] J. Paulose et al., *Nat. Phys.* 11 (2) (2015) 153–156.
- [268] Y. Huang et al., *Phys. Lett. A* 380 (13) (2016) 1334–1338.
- [269] G.W. Milton et al., *J. Eng. Mater.-T. ASME* 117 (4) (1995) 483–493.
- [270] J.N. Grima et al., *J. Mater. Sci.* 41 (10) (2006) 3193–3196.
- [271] J.N. Grima et al., *J. Non-Cryst. Solids* 356 (37) (2010) 1980–1987.
- [272] J.N. Grima et al., *Proc. Royal Soc. A* 468 (2139) (2011) 810–830.
- [273] N. Wicks et al., *J. Appl. Mech.* 71 (5) (2004) 652–662.
- [274] R.G. Hutchinson et al., *Int. J. Solids Struct.* 40 (25) (2003) 6969–6980.
- [275] K. Sun et al., *Proc. Natl. Acad. Sci.* 109 (31) (2012) 12369–12374. <https://doi.org/10.1073/pnas.1119941109>.
- [276] C.L. Kane et al., *Nat. Phys.* 10 (1) (2014) 39–45.
- [277] K. Sun et al., *Proc. Natl. Acad. Sci.* 109 (31) (2012) 12369–12374.
- [278] V. Vitelli, *Proc. Natl. Acad. Sci.* 109 (31) (2012) 12266–12267.
- [279] B.G. Chen et al., *Proc. Natl. Acad. Sci.* 111 (36) (2014) 13004–13009.
- [280] D. Yang et al., *Extreme Mech. Lett.* 6 (2016) 1–9.
- [281] Y. Bi et al., *Appl. Phys. Lett.* 112 (2018) 22.
- [282] Z. Zhang et al., *Compos. Struct.* 243 (2020) <https://doi.org/10.1016/j.compstruct.2020.112195>.
- [283] B. Berglund et al., *J. Acoust. Soc. Am.* 99 (5) (1996) 2985–3002. <https://doi.org/10.1121/1.414863>.